A THERMODYNAMIC MODEL OF A CENTRAL ARTIC OPEN LEAD

RICHARD HARRIS SCHAUS

United States
Naval Postgraduate School

THESIS

A Thermodynamic Model of a
Central Arctic Open Lead

by

Richard Harris Schaus

Thesis Advisor: J. A. Galt

September 1971

Approved for public release; distribution unlimited.

A Thermodynamic Model of a Central Arctic Open Lead

by

Richard Harris Schaus
Lieutenant Commander, United States Navy
B.S., University of Michigan, 1962

Submitted in partial fulfillment of the
requirements for the degree of

MASTER OF SCIENCE IN OCEANOGRAPHY

from the
NAVAL POSTGRADUATE SCHOOL
September 1971

ABSTRACT

A time-dependent, two-dimensional thermodynamic model of an open lead in central arctic sea ice is presented. The model is generated by opening a lead of finite width and infinite extent in the equilibrium sea-ice cover. From this initial condition, the model is integrated numerically as a sea-ice cover is reestablished over the lead. The effects of various representative advective parameterizations, and temperature and salinity profiles in the ocean's surface layer, on the heat flux through the lead and on the nature of ice formation are investigated as the lead closes by thermal processes alone. Continuity equations involving a horizontal advection term and a vertical diffusion term govern heat and salt transport in the water. Cooling-induced convective overturn as a mechanism for vertical heat and salt transport in the water column is treated through an artifice of the vertical diffusion term.

TABLE OF CONTENTS

LIST OF TABLES

LIST OF FIGURES

ACKNOWLEDGEMENTS

The topic for this thesis was suggested by Assistant Professor Jerry A. Galt of the Naval Postgraduate School, Monterey, California. His invaluable experience in the fields of arctic dynamics and the physical oceanography of the arctic, and his guidance in developing the conceptual model contributed greatly to the successful completion of the research. Associate Professor Warren W. Denner and Assistant Professor Ken L. Davidson, also of the Naval Postgraduate School, provided helpful ideas during the research. Associate Professor J. J. Von Schwind of the Naval Postgraduate School contributed valuable time and thought to reading the manuscript. To these people the author expresses his sincere thanks.

I. INTRODUCTION

A. POLAR AIR-SEA INTERACTIONS

Heat lost from polar regions together with the heat source of the tropics form the basis of the global general circulation. The flux of heat into polar regions from lower latitudes results from the general meridional temperature gradient from polar regions toward the equator due to unequal latitudinal heating of the earth's surface. Most of the heat advected into polar regions by the atmosphere is lost to space by long wave radiation, thus forming a basic mechanism for maintaining planetary radiative equilibrium.

Heat is also advected into polar regions by ocean currents, but due to the relative inefficiency of air-sea heat transfer and the relative slowness of ocean currents, this transfer is roughly one-tenth that attributed to the atmosphere.

Sea ice is a dominant feature of both arctic and antarctic seas; however, due to major differences in the physical configuration of sea and land masses of these regions, it plays decidedly different roles. The arctic, being essentially an ice-covered ocean, is extremely sensitive to climatic perturbations since the areal extent and depth of sea ice is critical to the regional energy balance. A surplus of about one-third of the annual energy influx would remove the arctic ice pack [Maykut and Untersteiner 1969, 1971]. On the other hand, the antarctic continental mass, covered by 2000 to 4000 meters of ice, is relatively insensitive to small energy flux perturbations, although its sea-ice cover would be affected similarly to that of the arctic.

Of major import to polar air-sea interactions is the degree to which the sea surface is covered by ice. Sea ice acts analogously to a 'lid' on the sea, modifying the dynamics and continuity of the sea and the air-sea system. Sea-ice cover dramatically reduces the heat transfer between ocean and atmosphere by effectively limiting that transfer to a process of molecular conduction. Further, by intercepting the vertical flux of momentum transferred from the mean wind field to the sea surface by the Reynold's stress, it suppresses wind mixing. Finally, it reflects a considerable portion of the incoming short-wave radiation, imposes an upper limit on the sea's surface-boundary temperature, reduces latent heat transfer by impeding evaporation, and, through its changes of phase, serves as a buffer, or damping mechanism. Alternatively, heat transfer processes are significantly enhanced over open-water areas in proximity to large ice masses, particularly during the winter, as surface air temperatures drop far below surface water temperatures. Wind and water stresses, in addition to directly affecting ocean-atmosphere heat transfer processes, keep the ice in nearly continuous motion, thus locally affecting heat transfer as well as producing mechanical stresses resulting in the formation of pressure ridges, polynya, and open leads.

Polar air-sea interactions are therefore characterized by complex feed back wherein the ocean and atmosphere individually and collectively influence the thickness and areal extent of the ice, which in turn has a pronounced effect on the exchange in question.

B. SURVEY OF PREVIOUS RESEARCH

Range and depth of interest in arctic research has expanded considerably since Nansen's epic drift in the FRAM (1893-1896). From pioneering studies

until only recently, research emphasis has been primarily of a descriptive nature, and it was not until the Soviet establishment of the drifting station "North Pole 1 (NP-1)" in 1937 that a systematic study of the arctic interior was initiated. Launching of a comparable long-range arctic research program by the United States would await the establishment of "Fletcher's Ice Island (T-3)" in 1952.

Attempts to understand the response of sea ice to environmental changes has long stimulated the interest of arctic researchers. Quantitative prediction of these responses has classically involved two primary approaches, the empirical and the theoretical. Although providing minimal insight to the dynamics of physical processes occurring between air, ice, and sea, empirical formulae relating sea-ice growth processes to observed surface temperatures have accomplished basic predictive goals. The most sophisticated example of this approach is perhaps one advanced by Bilello [1961]. Theoretical studies involved analytical solutions and were therefore severely limited in scope and complexity. One of the foremost of these analytical treatments is attributed to Kolesnikov [U.S. Naval Civil Engineering Laboratory 1966].

In the early 1950's the tenor of arctic research began to reflect increased emphasis on the theoretical approach to arctic dynamics as comprehensive data from systematic studies became available. It was at this point that studies relating the arctic energy balance to the mass budget and subsequent research directed toward heat transfer processes began to emerge. Development of physical relationships was confined to empirical and statistical approaches, or theoretical problems to which simple, analytical, approximate solutions could be developed.

Classic arctic heat budget studies were presented by several authors. Badgley [1961, 1966] summarized and collated available data to deduce a typical heat budget at the surface of the central Arctic Ocean. Fletcher [1966] discussed annual patterns of atmospheric heat loss for each component of the heat budget in relation to the general atmospheric circulation, for both ice-covered oceans and ice-free oceans. Vowinckel [Arctic Meteorology Research Group 1964] independently investigated the amount of heat conducted through the Arctic Ocean ice to check previously calculated values for the heat released from the Arctic Ocean. Doronin [1966] presented an analysis of heat-balance components of the surface layer in the Arctic Ocean. Coachman [1966] proposed a model to explain the observed features of the oceanic regime of the Arctic surface layer during the winter. Muench [Baffin Bay - North Water Project 1971] discussed the physical oceanography of the northern Baffin Bay region in considerable detail.

It was not until the 1960's and the attendant widened use of the high-speed digital computer as a research tool that physical processes could be modeled free of constraints imposed by analytical solutions. Using finite difference schemes, a system of integral-differential equations could now be solved rapidly within acceptable error limitations. Typical of first-generation numerical models in the field is that developed by Untersteiner [1966], which predicted thickness and temperature of sea ice, thus allowing further insight into the relationship of climatic change to ice production, ice decay, and equilibrium ice thickness. The advanced one-dimensional thermodynamic model of central Arctic sea ice developed by Maykut and Untersteiner [1969, 1971] is a prime example of the present theoretical approach.

C. PRESENT RESEARCH DIRECTION

A great deal of research effort is presently being directed toward developing numerical models of the atmosphere and of the ocean as well as atmosphere-ocean models, with the objective of ultimately producing an efficient, reliable global system model. Problems inherent in the realization of this objective are numerous and include not only a lack of refinement in respective models of the atmosphere and ocean, but also a lack of refinement in the technique of coupling the respective models. Further, observational input data is in general deficient for these models, particularly in the Arctic. Present state-of-the-art examples of models of this type are well represented by the sophisticated models of Manabe [1969] and Bryan [1969].

One of the more ambitious research projects in recent years is the Arctic Ice Dynamics Joint Experiment. AIDJEX is essentially a United States - Canadian cooperative effort to gain quantitative understanding of the interaction between atmospheric sea ice and fluid ocean fields of motion. In progress at the time of this writing, AIDJEX is unique in its observational approach since, in order to gain a full understanding of interacting fields, it involves the collaboration of many research groups in making coordinated measurements of interacting fields of motion, stress, and strain - observing appropriate time and space scales - over a minimum period of one year. The fruits of this ambitious and imaginative study, in terms of fresh insights, controlled data, and international cooperation appear to be vast already.

D. CONCEPTUALLY-RELATED STUDIES

Studies of Arctic dynamics, energy balances and mass budgets range over a wide spectrum. Scientific literature reflects numerous experimental and theoretical models of microstructure and micro-scale energy transfer processes between ocean and atmosphere, ice and atmosphere, and ice and ocean, essentially occurring in boundary-layer regions. Pertinent to the work presented herein is research performed by Foster [1968, 1969] in which haline convection induced by the freezing of sea water was studied, and by Lake and Lewis [1970] who studied salt rejection by sea ice during growth. Work performed by Lewis and Walker [1970] illustrates seasonal changes in the temperature and salinity profiles beneath annual sea ice cover, and Stern and Turner [1969] reported on the formation of salt fingers and convecting layers.

Directly related to the model proposed herein is the macroscale advanced model derived by Maykut and Untersteiner [1969, 1971] to forecast ice temperature and thickness, which defines the role of each component of the energy budget in relation to its effects upon the ice. Although comprehensive in its treatment of physical processes related to components of the energy budget, the model admittedly has several shortcomings. Physical limitations are due to uncertainties in environmental data and include the necessary assumption of a constant oceanic heat flux and generally course albedo and energy-flux data. Limitations, arising from an inability to model certain processes include: 1) the neglect of mechanical stresses produced by winds and surface currents, 2) treatment of turbulent fluxes at boundaries as being independent of growth rates or the physical states of ice and snow, 3) imprecise treatment of downward heat transport from

melting snow, 4) undefined shapes of salinity profiles for various ice conditions, and 5) neglect of heat storage by melt ponds. Leads were considered only so far as they indirectly affected the energy fluxes over the bare ice. In spite of its limitations, this will certainly be a cornerstone for future thermodynamic ice models and provides a number of conceptual bridges used in the present work.

E. THESIS OBJECTIVE

It is known that significant heat transfer occurs between the atmosphere and the ocean through open leads in the Arctic sea ice cover. As found experimentally by Badgley [1961], sensible heat loss is at least two orders of magnitude greater from open leads than from perennial sea ice.

With the need for further refinement in models of the ocean and the atmosphere, as well as in model coupling schemes, the requirement for mesoscale examination of ocean-ice-atmosphere heat-transfer processes is immediate and apparent. With appropriate observational input data becoming increasingly more abundant, informative numerical models of mesoscale processes appear promising for furthering the understanding of physical processes and for realizing control of mass-energy fluxes in the arctic.

The objective of this study was to develop a thermodynamic model of an open lead in central arctic sea-ice in which hydrodynamic processes of convection, advection, and diffusion of heat and salt were represented. By integrating the model numerically, the effects of various representative advective parametizations, and temperature and salinity profiles in the ocean's surface layer, on the heat flux through the lead and on the nature of ice formation, could be investigated as the lead reclosed by thermal processes alone.

II. NATURE OF THE PROBLEM

Since sea ice essentially insulates the ocean from the atmosphere and suppresses important thermodynamic processes, it, along with heat-advecting ocean currents, becomes a primary factor in determining the vertical structure in Arctic seas. However, the dynamic transition from ice-free to ice-covered seas is not fully understood. In particular, the nature of the fluxes of salt and heat, as well as the structure and depth of unstable convective overturn during initial phases of the freezing process, require study.

A. DYNAMICS OF THE SEA WATER FREEZING PROCESS

The structure of the active surface layer of the Arctic Ocean is generally horizontally uniform with a very stable density gradient. However, during the freezing process the density gradient may be significantly altered by three primary mechanism: 1) progressive cooling of surface waters from above, 2) brine expulsion by the ice during the freezing process, and 3) advection of heat and/or salt by surface currents.

The fundamental physical relation which makes the sea water freezing process unique may be understood by examining the curves of maximum density and freezing point for sea water, plotted with respect to temperature versus chlorinity or salinity (Figure 1). Specifically, for waters of salinity greater than 24.70 parts per thousand, the temperature of maximum density of the liquid state will always be lower than the liquid's freezing-point temperature under pressures existing in nature. Any process that tends to produce a vertical density instability will induce convective overturn in

Figure 1.
Temperatures of Sea Water
Maximum Density and
Freezing-Point
vs
Chlorinity

*after Sverdrup, Johnson and Fleming [1942]

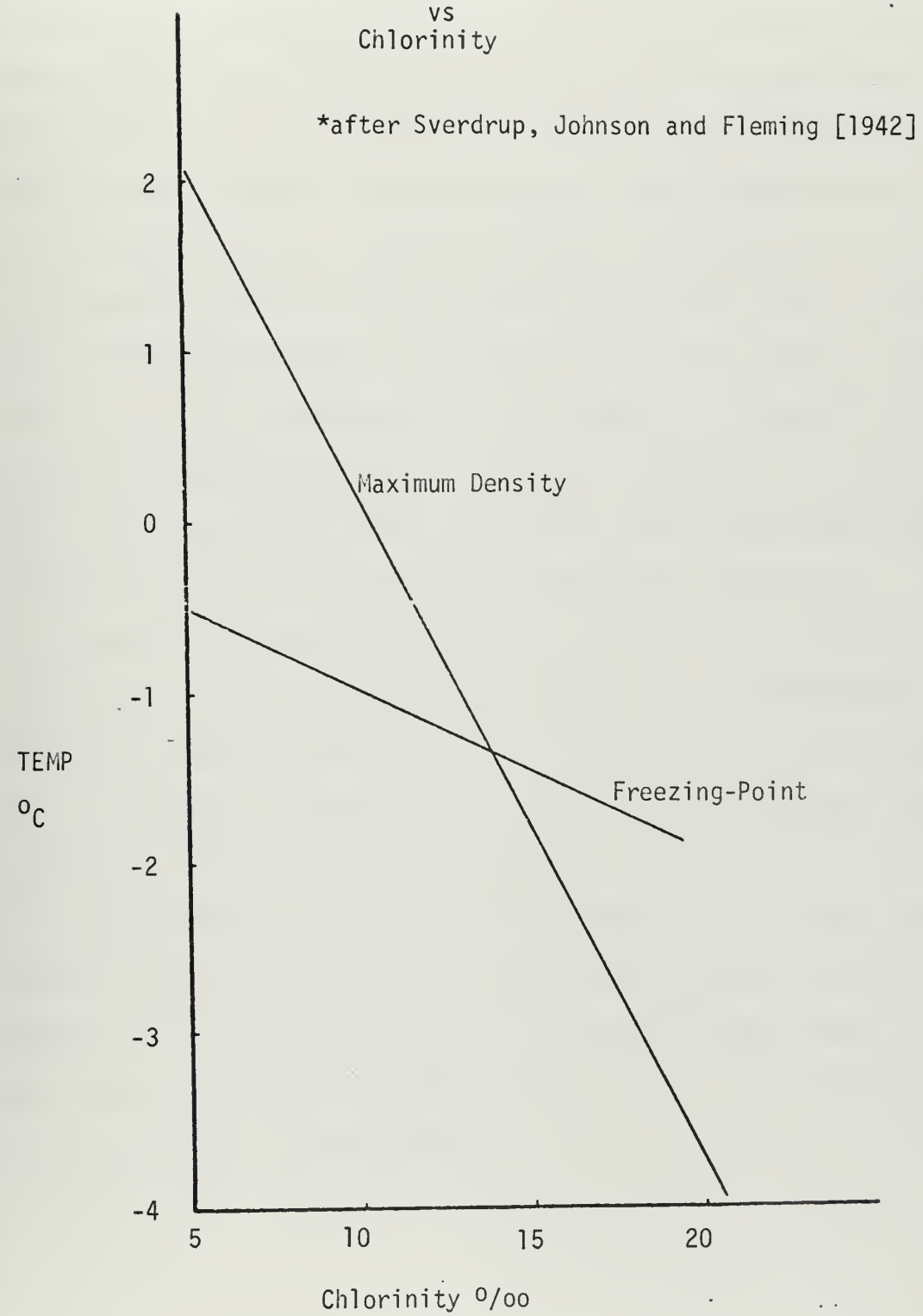

the water column, resulting in mixing of the unstable segment such as would be produced in the freezing process by surface cooling and freezing-associated brine expulsion. Convective overturn will therefore be continuous in the unstable segment of the liquid water column from the onset of surface cooling to the point of total change-of-phase of the water column. A somewhat less obvious but straightforward point should be mentioned in qualification of the foregoing. From an arbitrary water temperature above the freezing point, down to, but not including the freezing point, convection is temperature controlled during cooling since there is no ice formed, hence, no brine expulsion. During cooling of surface waters at the freezing point for existing surface salinities, convection is primarily salinity controlled since brine is being continuously expelled from newly forming ice. Within this latter water temperature regime, temperature changes play a minor role in effecting changes in surface water densities.

As convective overturn is a mechanism for inhibiting freezing by continuously transferring heat from depth to the active boundary at which freezing is taking place, so it is also a mechanism for effectively removing heat from depths significantly greater than could be effected by molecular diffusion. An equilibrium ice thickness is reached when the resultant heat flux upward through convection, advection and diffusion in the water column balances the upward resultant heat flux through the ice, at the ice-water boundary. Prior to this point, ice is accreted in depth since the upward heat flux through the ice exceeds the upward heat flux in the water column arriving at the ice-water boundary.

B. DISTRIBUTION OF VARIABLES

The distribution of temperature, salinity and velocity are considered within a volume of water under a refreezing lead. The water is assumed to be inviscid, horizontally homogeneous, horizontally isotropic, irrotational, and incompressible. Accelerations resulting from the coriolis effect and horizontal pressure gradients are assumed to be negligible. Momentum, heat energy, and salt mass are conserved within the volume such that no velocity, temperature, or salinity sources or sinks exist except at the volume's boundaries. Furthermore, currents are assumed to be steady-state and uniform both horizontally and vertically.

Using the classic box-model approach, these conservative fields are represented continuously within the volume by individual continuity equations. For the vector field of velocity, where K is the diffusivity and S_v is a source term,

$$D\mathbf{V}/_{Dt} = \nabla \cdot K \nabla \mathbf{V} + S_v \tag{1}$$

which reduces to

$$\mathbf{v}(t,x,y,z) = \mathbf{V} = \text{constant} \tag{2}$$

i.e., the velocity is specified as uniform and steady.

Similarly, the scalar fields of heat and salt, here collectively depicted by the scalar quantity $\emptyset$, are represented by

$$D\emptyset/_{Dt} = \nabla \cdot K \nabla \emptyset + S_{\emptyset} \tag{3}$$

where K is the diffusivity and $S_{\emptyset}$ is a source term.

This reduces to

$$\partial\phi/\partial t = - \mathbf{v} \cdot \nabla\phi + K_H \nabla^2\phi + \nabla_v \cdot K(z) \nabla_v\phi \qquad (4)$$

where K_H is the horizontal diffusivity and ∇_v is the vertical del operator since,

$$K(x) = K(y) = K_H = \text{constant}$$

$$S_\phi = 0 \quad .$$

The local, or time-rate-of-change, is therefore equal to the sum of the field-rate-of-change and the diffusive-rate-of-change.

C. HYDRODYNAMIC PROCESSES

Mechanisms for the hydrodynamic transport of heat and salt within the lead are advection and diffusion. However, from the dynamics of the sea-water freezing process, it is known that convection plays a major role in transporting both heat and salt in the water column. Although it is not represented by a discrete term in the foregoing continuity equation, the convective transport term may be thought of as simply a temporary (when vertical density instabilities arise) modification of the vertical diffusion term taking the form

$$\lim_{K(z)\to\infty} \partial/\partial z \; K(z) \; \partial\phi/\partial z \qquad (5)$$

which in essence results in free vertical (convective) transport.

D. MASS AND ENERGY BALANCE

With the foregoing analyses of continuity relations and mechanisms of hydrodynamic transport existing within the box model of the open lead, the mass and energy balances existing at the volume's boundaries may be examined.

Over an arbitrary surface area of a reclosing lead, a given change of heat, ΔQ, at the water surface must equal the heat added by advection and diffusion at upstream boundaries, Q_u, plus the heat added from depth in the lead by convection, advection, and diffusion, Q_z, plus the heat added by surface ice accretion, Q_f, plus the open-water heat loss at the surface by conduction, evaporation and radiation, $Q_s+Q_e+Q_r$, plus the heat loss through the ice cover by conduction, Q_i, minus the heat diffused across vertical boundaries normal to advective transport, Q_n, minus the heat transported across the downstream boundaries by advection and diffusion, Q_d, such that

$$\Delta Q = Q_u + Q_z + Q_f + W(Q_s+Q_e+Q_r) + Q_i(1-W) - Q_n - Q_d \qquad (6)$$

Where W is the fraction of open water comprising the surface of the lead at any given time. The heat added from depth in the lead is heat ultimately derived from the Bering Sea Water (in the Canadian Basin) and from the Atlantic layer.

By similar analysis, a given change of salinity, ΔS, at the water's surface must equal the salt added by advection and diffusion at upstream boundaries, S_u, plus the salt added from depth in the lead by convection, advection, and diffusion, S_z, plus the salt added by surface ice accretion (salt rejection), S_f, plus the salt lost through surface ice melting (salt dilution), S_m, plus the salt added by surface evaporation, S_e, minus the salt diffused across vertical boundaries normal to advective transport, S_n, minus the salt transported across downstream boundaries by advection and diffusion, S_d, such that

$$\Delta S = S_u + S_z + (1-W)(S_f+S_m) + W(S_e) - S_n - S_d \qquad (7)$$

where again W is the fraction of open water comprising the surface of the lead at any given time. The salt added from depth in the lead is derived from the generally strong positive halocline existing at depths below 25 to 50 meters.

Qualitatively then, before the equilibrium sea ice cover has been reestablished, there will exist differentials in the temperature and salinity profiles of water columns. A primary process of interest in the refreezing lead is that of surface ice formation, which lends a unique character to lead hydrodynamics. The heat added/lost by surface ice accretion/melting is a function of the incremental change in the mass of ice, ΔI, and the heat of formation of sea ice, L_i, such that

$$Q_f = -Q_m = L_i \cdot \Delta I \tag{8}$$

Coupled directly to this process is the process of brine expulsion (salt rejection) by the sea ice during growth. The salt added/lost by surface ice accretion/melting is a function of the incremental change in the mass of ice, ΔI, the salinity of the sea ice, S_i, (which in turn is dependent upon rate-of-freezing, ice temperature, and age of the ice), and the salinity of the parent sea water, S_w, such that

$$S_f = -S_m = f(\Delta I, S_i, S_w) \tag{9}$$

Qualitative analysis of the salt rejection process by constituent salts is not appropos to either the scale or the nature of the study at hand; therefore salt rejection was treated simply as a process of water-salinity modification.

III. EXPERIMENTAL PROCEDURE

A. FORMULATION OF THE MODEL

1. Establishment of a Representative Cross Section

In deciding upon what physical dimensions would be appropriate for the model, it appeared most suitable to represent a small open lead in central arctic sea ice such as one would expect to observe between early to late winter. Therefore, the width of the lead was chosen to be 150 meters, with an additional 50 meters under equilibrium sea-ice cover on the downstream side of the model lead to facilitate studying resultant thermodynamics and hydrodynamics in that region.

The model's depth extent was set at 50 meters based upon lower boundary condition considerations. Over much of the Arctic Basin the vertical temperature gradient at that depth is zero or very slightly positive. Since a no-flux lower boundary condition was desirable in order to better study the effects of advection of conservative constituents in the lead, that depth was chosen.

It was felt that the model could be simplified without the loss of any essential physics if derivatives along the lead (Y-axis) were set to zero. This reduced the problem to one of looking at a cross-sectional distribution in the lead. Figure 2 is a pictorial depiction of the open lead.

2. Adaptation of the Continuity Equations to the Model

Using the simplification of the previous paragraph which allows the use of a cross-sectional area rather than a true volume to represent the

Figure 2.

Pictorial Depiction of Open Lead

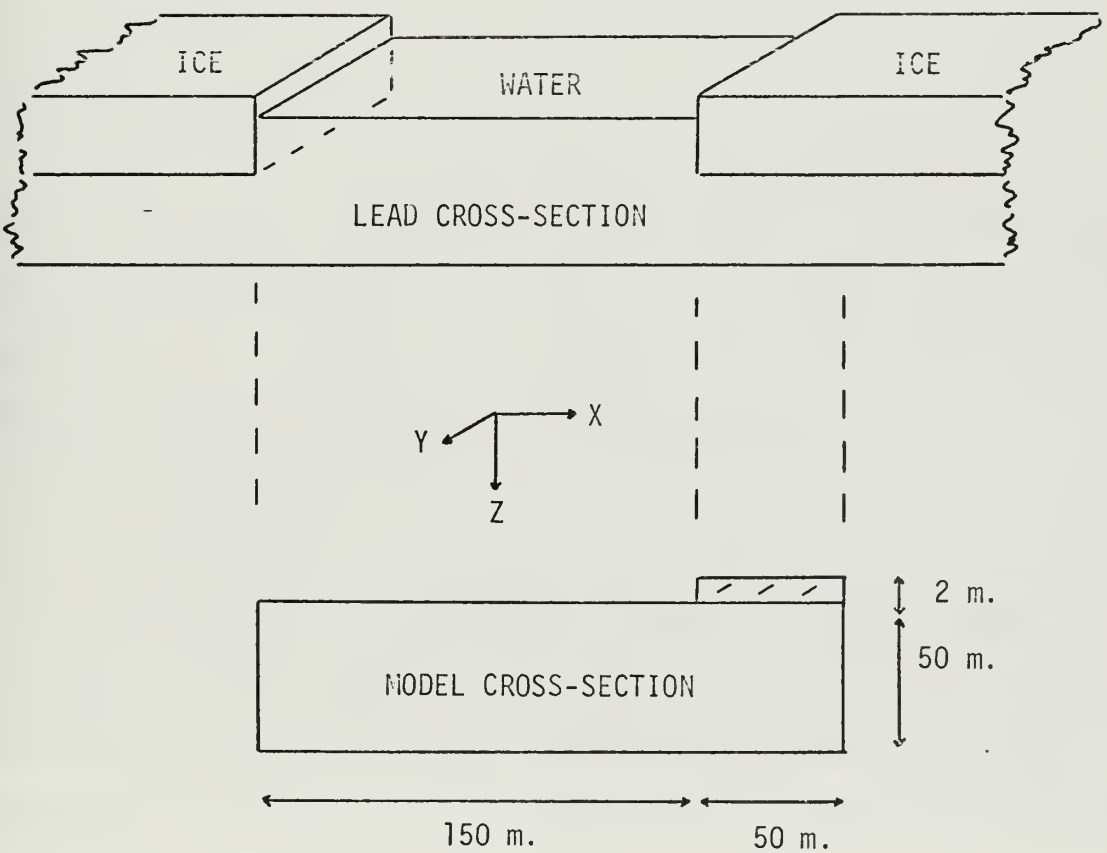

lead, the horizontal advection and horizontal diffusion terms describing changes along the Y-axis were eliminated from equation (4).

The problem was further simplified by assuming that all horizontal diffusion was negligible relative to horizontal advection, and that vertical advection could be disregarded.

Applying the foregoing simplifications to the expanded form of equation (4), and choosing the state variables of temperature and salinity as the relevant dependent variables, the final form of the equations used to describe the conservative scalar fields of temperature and salinity within the lead was

$$\partial \phi / \partial t = - u \, \partial \phi / \partial x + \partial / \partial z \; K(z) \, \partial \phi / \partial z \qquad (10)$$

where,

$$\phi = \phi \; (t,x,z)$$

3. Initial Conditions

Sea-water temperatures and salinities within the lead at the instant that the lead is generated are represented by local stable temperature and salinity profiles previously existing beneath the equilibrium sea-ice cover. The temperature and salinity fields are both horizontally uniform and vary only with depth in the lead such that

$$T(0,X,Z) = T(Z) \qquad (11)$$

$$S(0,X,Z) = S(Z) \qquad (12)$$

The surface of the newly-generated lead is initially taken to be ice-free over the left (upstream) 150 meters, and ice-covered with equiligrium thickness ice over the right (down-stream) 50 meters. Surface temperatures are initially at the freezing point, in temperature equilibrium with the preexisting sea-ice cover.

4. Boundary Conditions

The model's left, or upstream boundary, may be regarded as a source boundary across which sea water having a given temperature and salinity profile flows into the lead. Sea-water temperature and salinity profiles are taken as steady-state functions of depth alone, identical to the lead's initial temperature and salinity profiles such that

$$T(t,0,Z) = T(Z) \tag{13}$$

$$S(t,0,Z) = S(Z) \tag{14}$$

The model's surface boundary is the primary region of mass and energy fluxes and is therefore the most dynamically active boundary. The boundary condition on temperature across the entire surface is that of an upward (or downward) diffusive flux of heat across the water surface such that

$$\partial/\partial_z \, T(t,X,0) = f(\Delta T, Z_i, S_i, K_W, K_i) \tag{15}$$

where ΔT is the air-water temperature difference (an externally specified parameter), Z_i is the surface ice thickness, S_i is the surface ice salinity (an externally specified constant parameter), and K_W and K_i are the coefficients of thermal eddy diffusivity of sea water and thermal conductivity of sea ice respectively. When no ice is present at the surface, the surface heat flux is taken as the cumulative open-water sensible, latent, and radiative heat fluxes, which are specified in the model as external parameters according to the air-water temperature difference. Since the model's surface at all times represents the water surface, the fluxes at that boundary are matched as ice is formed, such that the flux through the water surface is always equal to the flux through the ice to the atmosphere, but at no time does it exceed the maximum open-water flux to the atmosphere.

The boundary condition on sea water salinity at the surface specifies a no-diffusive flux condition between air and water as well as between ice and water and ice and air such that

$$\partial/\partial_z \; S(t,x,o) \quad = 0 \tag{16}$$

However, salt rejection from ice to water during the freezing process (as well as salt dilution during melting) is represented as a discrete process of physically adding the change in salinity produced by sea-ice accretion or melting to the surface waters such that

$$S(t,x,o) \Rightarrow S(t,x,o) + \quad f(\Delta I, \Delta S) \tag{17}$$

where ΔI is the incremental change in the mass of sea ice, and ΔS is the salinity differential existing between the sea ice and its parent sea water.

The bottom boundary, as previously discussed, is characterized as a no-flux boundary, thus

$$\partial/\partial_z \; T(t,X,h) \quad = 0 \tag{18}$$

$$\partial/\partial_z \; S(t,X,h) \quad = 0 \tag{19}$$

where h is the model's depth extent.

The right, or downstream boundary, is also characterized as a no-diffusive flux boundary where whatever temperature-salinity field is generated by the thermodynamic processes of the lead is simply advected out. However, as mentioned previously, the right 50 meters of the lead model's surface is overlain by an equilibrium sea-ice cover. This boundary condition is therefore representative of a return towards the equilibrium vertical profiles. At the model's right boundary then

$$\partial/\partial X \; T(t,W,Z) = 0 \qquad (20)$$

$$\partial/\partial X \; S(t,W,Z) = 0 \qquad (21)$$

where W is the model's width.

Figure 3 describes processes considered in the model cross section. Figure 4 schematically represents the model cross section with its governing continuity equations and boundary conditions. In this figure, the surface boundary condition is simply a statement of the balance of fluxes at the ice-water boundary. With no ice cover ($\delta = 0$), the upward heat flux through the water surface, F_Σ is equal to the sum of open-water sensible (F_s), latent (F_e), and radiative (F_r) heat fluxes. When an ice cover is present ($\delta > 0$), the upward heat flux through the water surface ($z = 0^+$) is equal to the upward heat flux through the ice ($z = 0^-$) minus the heat added by surface ice accretion. The above relations are presented in terms of temperature gradients in Figure 4 as they are applied to the governing continuity equation for temperature. Symbols not previously defined are ρ_i, volume density of sea ice; q_i, heat of formation of sea ice; δ ice thickness (volume of ice per unit surface area).

5. The Finite-Difference Scheme

A purely explicit finite difference scheme was selected to numerically represent the linear parabolic partial differential equation (10). The time rate-of-change term was represented by forward differencing, the field rate-of-change term by backward (upstream) differencing, and the diffusive rate-of change term by central differencing. Thus over the interior (non-boundary) region of the model

$$\frac{\phi^{n+1}_{j,k} - \phi^{n}_{j,k}}{\Delta t} = - \frac{\phi^{n}_{j,k} - \phi^{n}_{j-1,k}}{\Delta x} + K \frac{\phi^{n}_{j,k+1} - 2\phi^{n}_{j,k} + \phi^{n}_{j,k-1}}{(\Delta z)2} \qquad (22)$$

Figure 3.

Description of Processes Considered in Model

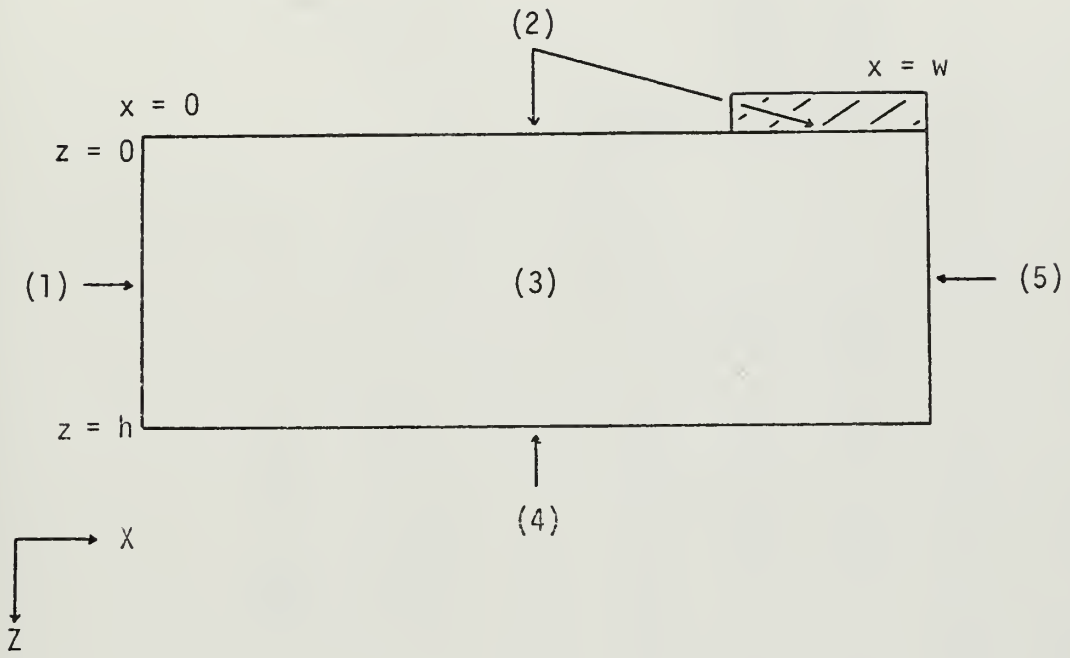

(1) Advection of steady-state temperature-salinity field into the lead from under equilibrium ice pack.

(2) Heat loss to the atmosphere as a function of ice thickness, ice accretion/melting, and salt rejection/dilution.

(3) Heat and salt transport by convective overturn, advection and eddy diffusion.

(4) No transport across boundary.

(5) Advection of temperature-salinity field generated by lead thermodynamics out of the lead model.

Figure 4.
Model Cross Section with Governing Continuity Equations and Boundary Conditions.

$$\frac{\partial}{\partial Z} T\{t,x,o^+\} = \begin{cases} \dfrac{F_\Sigma}{K_w} & , \delta = 0 \\ \dfrac{K_i}{K_w} \dfrac{\partial}{\partial Z} T\{t,x,o^-\} - \dfrac{\rho_i q_i}{K_w} \dfrac{\partial \delta}{\partial t} & , \delta > 0 \end{cases}$$

$$\frac{\partial}{\partial Z} S\{t,x,o^+\} = 0$$

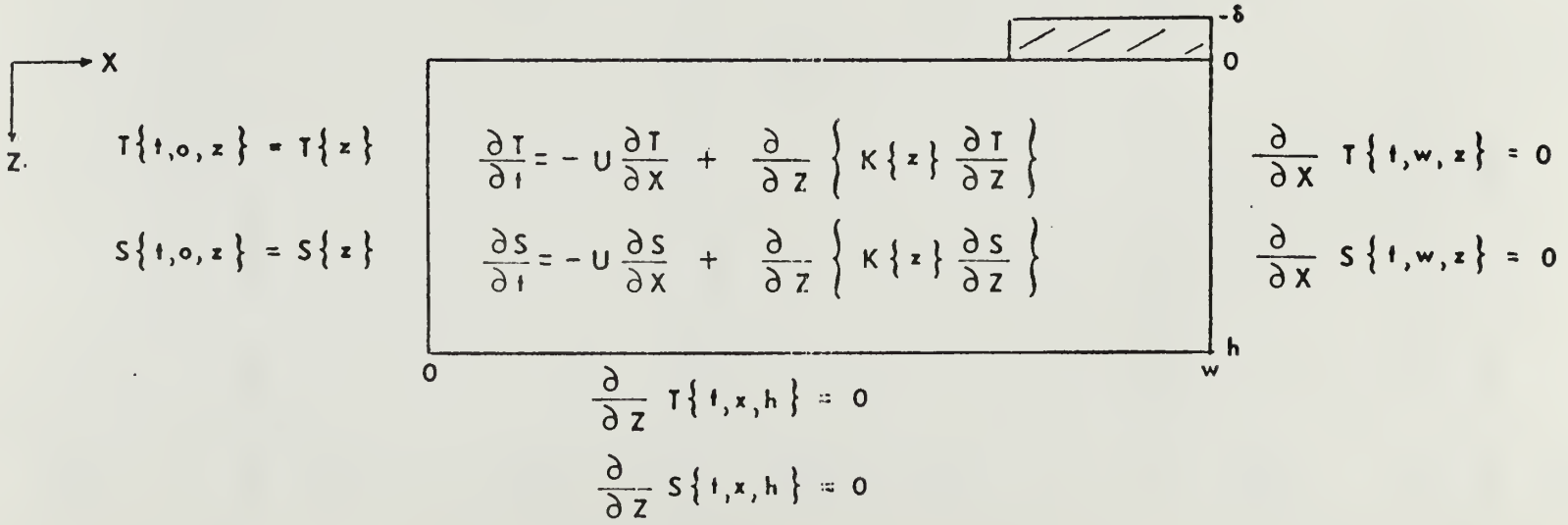

where,

$$\phi^{n}_{j,k} = \phi^{n\Delta t}_{j\Delta x,\ k\Delta z} \tag{23}$$

At the left boundary, equation (22) was inapplicable since temperature and salinity were both steady-state functions of depth alone. Therefore, at this boundary at all times

$$\phi^{n+1}_{j,k} = \phi^{n}_{j,k} \tag{24}$$

At the surface boundary, the diffusive term for temperature was modified in equation (22) since

$$\frac{T^{n}_{j,k+1} - T^{n}_{j,k-1}}{2\Delta Z} = \nabla_{v} T \tag{25}$$

or,

$$T^{n}_{j,k-1} = T^{n}_{j,k+1} - 2\Delta Z(\nabla_{v} T) \tag{26}$$

The diffusive salt term at the surface was modified in equation (22) since

$$\frac{S^{n}_{j,k+1} - S^{n}_{j,k-1}}{2\Delta Z} = 0 \tag{27}$$

or,

$$S^{n}_{j,k-1} = S^{n}_{j,k+1} \tag{28}$$

At the bottom boundary, the diffusive rate-of-change terms of both temperature and salinity were modified in equation (22) since

$$\frac{\phi^{n}_{j,k+1} - \phi^{n}_{j,k-1}}{2\Delta Z} = 0 \tag{29}$$

or,

$$\phi^{n}_{j,k+1} = \phi^{n}_{j,k-1} \tag{30}$$

Finally, at the right boundary, equation (22) remains unmodified since advection is the only transport mechanism operating across it.

Stability analysis of the finite difference equation using the Fourier series method [Smith 1965] shows that

$$\epsilon^{n+1}_{j,k} = \epsilon^{n}_{j,k}\left[\Delta t\left\{\frac{U}{\Delta x} + 2\,\frac{K}{(\Delta z)^2}\right\}\right] \tag{31}$$

where ϵ represents an arbitrary error introduced into the problem. Therefore, the finite-difference equation (22) is stable when the absolute value of the amplification factor remains less than or equal to unity

$$\left|\Delta t\left\{\frac{U}{\Delta x} + 2\,\frac{K}{(\Delta z)^2}\right\}\right| \leq 1 \tag{32}$$

6. Representation of Physical Processes

Convective overturn is treated nominally through an artifice of the vertical diffusion term as in equation (5). Numerically however, convective overturn and its associated mixing is accomplished through arithmetic averaging of temperatures and salinities within regions of vertical density instability as determined by sigma-t values, followed by recomputation of the resultant sigma-t value for the newly mixed (and neutrally stable) region. Subroutine OVRTRN accomplishes convective overturn in the model.

Advection of heat and salt (temperature and salinity) in the lead is driven by a current, u, in the positive-x direction. Values and depth profiles of the current as used in the model are given in subparagraph B of this section.

Diffusion of heat and salt in the vertical are determined by the coefficients of vertical temperature and salinity diffusivities, both set at constant values of 10 cm^2 sec^{-1} in the model.

Formation of sea ice is accomplished as in equation (8). More specifically however, when a given mass of water, Δw, is cooled ΔT degrees centigrade below its salinity dependent freezing-point temperature, the incremental mass of ice formed, ΔI, is

$$\Delta I = {}^{C_p(\Delta W \cdot \Delta T)}/_{L_i} \qquad (33)$$

where C_p is the specific heat of sea water and L_i is the heat of formation of sea ice.

Salt rejection (or dilution) resulting from surface sea ice accretion (or melting) is described in equation (17). Specifically, if ΔI is the incremental change in the mass of sea ice and ΔS is the salinity differential existing between a unit mass of parent sea water and a unit mass of its generated sea ice, then the incremental salinity change, ΔS_R, in the surface waters resulting from that freezing or melting process is

$$\Delta S_R = \Delta I \cdot \Delta S \qquad (34)$$

7. Physical Quantities and Relations

Sea water chlorinity is related to salinity [Knudsen 1902] by the relation

$$Cl = (S - 0.030)/1.8050 \qquad (35)$$

Freezing-point depression is empirically related to sea water chlorinity by Thompson [Sverdrup, Johnson and Fleming 1942] by the relation

$$T_{fp} = -0.0966 \cdot Cl - 0.0000052 \cdot Cl^3 \qquad (36)$$

The density of sea water as a function of salinity and temperature (sigma-t) [Knudsen 1902] is empirically computed through

$$\sigma_o = f_1(Cl) \tag{37}$$

$$A_T = f_2(T) \tag{38}$$

$$B_T = f_3(T) \tag{39}$$

$$\Sigma_T = f_4(T) \tag{40}$$

$$\sigma_t = f_5(\Sigma_T, \sigma_o, A_T, B_T) \tag{41}$$

The specific heat at constant pressure of sea water is empirically related to its salinity at normal temperature and pressure by Kuwahara [Sverdrup, Johnson and Fleming 1942] by the relation

$$C_p = 1.005 - 0.004136 \cdot S + 0.0001098 \cdot S^2 - 0.000001324 \cdot S^3 \tag{42}$$

The thermal conductivity of sea ice was determined using the relationship established by Untersteiner [Maykut and Untersteiner 1969, 1971].

$$k_i = k_f + \frac{B \cdot S(z)}{T} \quad , T<0 \tag{43}$$

where,

the subscript f refers to pure ice,

$k_f = 0.00486$ cal/cm-sec-^oC,

$B = 0.28$ cal-cm^2/g-sec,

T = temperature of ice in degrees Celsius,

$S(z)$ = ice salinity at depth z in g/cm^3.

The heat of formation of sea ice was represented by the simplified relationship [Pounder 1965]

$$L_i \doteq L_f \cdot (1 - \frac{\sigma}{S}) \tag{44}$$

where,

$L_f = 79.77$ cal/g,

σ = salinity of sea ice, g/kg,

S = salinity of parent sea water, g/kg.

B. ENVIRONMENTAL DATA INPUTS

Environmental data used in the model fell into two basic categories: that which remained constant throughout all runs of the model, and that which was variable from run-to-run. Representative of the former were initial equilibrium-ice thickness, set at 200 cm, an ice salinity of 8.0 g/kg, and an ice density of 0.91 g/cm^3. Further, representative open water sensible, latent, and radiative heat flux densities as presented by Muench [Baffin Bay-North Water Project 1971] were applied in the model. However, as ice formed at the surface, the latent heat flux density was modified so as to decrease exponentially with increasing ice thickness. The radiative heat flux density was modified so as to decrease from open water values as ice formed, approaching a constant value representative of the radiative flux density over pack ice as also presented by Muench. The sensible heat flux density was modified internally by the relation shown in Figure 4 as surface ice thicknesses increased. All surface heat flux densities were representative of an air-water temperature difference of $25^{o}C$ with no wind. Finally, the coefficients of vertical temperature and salinity eddy diffusivity were set at 10.0 cm^2/ sec.

Primary variable parameters in the model were horizontal current magnitudes, vertical temperature profiles, and vertical salinity profiles. Currents applied in the model were within the range of zero to 10.0 cm/sec. Extreme test case values were 0.0 and 10.0 cm/sec. Additional test case values of 2.0 and 4.0 cm/sec were used to study one particular temperature-salinity field combination with its associated hydrodynamics in further detail. A value of 7.0 cm/sec was chosen to represent a typical horizontal current occurring in the lead, and was subsequently used as the real case value.

Test case values of vertical temperature and salinity profiles representative of extremes in vertical gradient were applied. Profiles A represented strong gradients, while profiles B represented weak gradients (Table I). Real case temperature and salinity profiles, qualitatively representative of early winter (profile C) and late winter (profile D) conditions in the central arctic [Coachman and Barnes 1961, 1962], were chosen to represent the typical lead.

Table I summarizes the profile designations of the three variable parameters and their various values.

C. MODEL INTEGRATION PLAN

In order to gain maximum insight to physical processes occurring in the lead, as well as to study the effects of current magnitude, vertical temperature gradient, and vertical salinity gradient on lead thermodynamics, the series of test variables was run in the model. Represented by runs one through eight, these test cases involved running all possible combinations of current magnitude (u) profiles A and B, temperature (T) profiles A and B, and salinity (S) profiles A and B. These test cases were integrated over a lead reclosure period of two days.

As a result of the interesting dynamics occurring in run 6, additional runs 9, 10, and 14 were scheduled using temperature and salinity profiles identical to run 6 (and 2), but with current magnitude profiles C, D, and F respectively, in order to further investigate these phenomena. Integration was again for a period of two days.

Finally, the real-case variables, representative of naturally occurring parameters, were put into the model and integrated over two-day periods in runs 11 and 12, and over a 30 day period in run 13.

Table I. Environmental Variable Profiles

Horizontal Current Magnitudes (cm/sec)

Depth (m)	Profile					
	A	B	C	D	E	F
0 - 50	10.0	1.0	2.0	4.0	7.0	0.0

Water Temperatures (°C)

Depth (m)	Profile			
	A	B	C	D
0	-1.50	-1.50	-1.68	-1.82
5	-1.40	-1.49	-1.68	-1.82
10	-1.30	-1.48	-1.68	-1.82
15	-1.20	-1.47	-1.67	-1.82
20	-1.10	-1.46	-1.66	-1.81
25	-1.00	-1.45	-1.65	-1.80
30	-0.90	-1.44	-1.64	-1.79
35	-0.80	-1.43	-1.63	-1.78
40	-0.70	-1.42	-1.62	-1.77
45	-0.60	-1.41	-1.61	-1.76
50	-0.50	-1.40	-1.60	-1.75

Water Salinities (g/kg)

Depth (m)	Profile			
	A	B	C	D
0	28.00	28.00	31.00	33.51
5	28.50	28.01	31.01	33.52
10	29.00	28.02	31.02	33.53
15	29.50	28.03	31.06	33.55
20	30.00	28.04	31.15	33.57
25	30.50	28.05	31.25	33.60
30	31.00	28.06	31.35	33.63
35	31.50	28.07	31.45	33.66
40	32.00	28.08	31.55	33.69
45	32.50	28.09	31.65	33.72
50	33.00	28.10	31.75	33.75

Table II presents a summary of runs conducted with their respective variable combinations.

D. MODEL LIMITATIONS

In addition to the assumptions made earlier in arriving at the simplified model of an open lead, basic limitations in the model's capabilities are: 1) the atmosphere is treated as an external parameter such that it affects lead dynamics but cannot be affected in turn by the lead; 2) sea ice is treated as a quasiexternal parameter since it is depicted as a simple, uniform mass floating on the water's surface. Density and salinity are constant throughout this mass in both space and time, and the vertical temperature gradient is taken to be linear throughout. Its thermal conductivity is determined only at the ice-water boundary, which is warmest and therefore limiting through the relation given in equation (43), and an upper limit is applied to the upward heat-flux density through the ice such that at no time is the flux through the ice allowed to exceed that over open water; 3) mechanical lead closure (such as by wind-drifted ice) is disallowed; 4) snow cover over the lead's surface is not modelled; 5) super-cooling of surface waters [Coachman 1966] is not portrayed; 6) as convection-induced mixing occurs instantaneously in the model, so also does surface ice melting whenever heat is brought to the surface by convection. This results in an artificiality in that, although heat and salt are conserved in the model, heat brought to the surface under an ice cover immediately melts ice until no further surface heat is available for melting. Therefore, under this limitation, it is not possible for surface heat to be advected downstream under an ice cover to promote downstream melting. Only in cases when no ice is present to be melted may this heat

Table II. Schedule of Runs and Variable Combinations

Run	Variable Profile			Period of Integration (days)
	U	T	S	
1	A	A	A	2
2	A	A	B	2
3	A	B	A	2
4	A	B	B	2
5	B	A	A	2
6	B	A	B	2
7	B	B	A	2
8	B	B	B	2
9	C	A	B	2
10	D	A	B	2
11	E	C	C	2
12	E	D	D	2
13	E	D	D	30
14	F	A	B	2

be advected downstream; 7) in situations wherein vertical salinity gradients existing in the water column are weaker than a certain minimum gradient, the model will over-mix the water column in depth. Specifically, the model forms ice in response to surface cooling, thereby rejecting salt into the surface water layer of depth Z. The model then mixes the induced unstable region as determined by relative sigma-t values of density. If however, there is heat available at some shallower depth than that to which the water column was mixed which could have decreased the initial amount of ice formed, then although salt, ice, and heat are ultimately conserved, potential energy is not conserved. Initial freezing and resultant salt rejection have induced convection to a greater depth than would have actually been the case in a continuous process. Therefore, for vertical salinity gradients weaker than a certain minimum gradient, the model's numerical convective process acts as a potential energy source. Quantitatively, the limiting minimum vertical salinity gradient which can be accurately treated by this model, in g/kg per vertical grid space, is

$$\rho_i \cdot (S_w - S_i) \cdot \Delta I / \Delta Z \qquad (45)$$

where ρ_i is the ice density, S_w is the salinity of sea water, S_i is the salinity of sea ice, ΔI is the incremental change in the volume of ice, and ΔZ is the vertical grid spacing. In this model, the limiting gradient is in the neighborhood of 1×10^{-3} g/kg per vertical grid space, which is lower by an order of magnitude than the weakest salinity gradient used.

IV. PRESENTATION OF DATA

Some results of integrating the model using the combinations of environmental variables summarized in sections III.B. and III.C. are presented in tabular and graphic form. Three primary output variables are treated: surface ice thickness, surface heat loss to the atmosphere, and depth of penetration of surface-freezing induced convective overturn. Throughout the section, these three output variables are related by run number (section III.C.) to the input variables of current magnitude, vertical temperature profile and vertical salinity profile (section III.B.).

A. TEST CASES

Ice thicknesses are treated in two ways: by time growth rate and by spatial profile across the lead. Values for growth rates were arrived at by tabulating the maximum ice thickness occurring anywhere in the lead as a function of time. Values for spatial profiles were taken as the ice thicknesses across the model's surface (200 meters) after 48 hours of freezing. Values over the right 50 meters of the model's surface, initially covered by 200 cm of ice, are tabulated to show the downstream surface effects of lead thermodynamics on the equilibrium ice cover.

Surface heat losses to the atmosphere are presented as cumulative heat-loss densities (heat loss per unit surface area) occurring at each grid point over the surface of the initially open lead after 48 hours of lead reclosure. Additionally, these surface heat-loss densities are averaged and tabulated separately as mean surface heat-loss densities.

Finally, maximum depths of penetration of surface-freezing induced convective overturn are tabulated. Due to the numerical nature of the model however, these depths should be treated as bounding depths rather than precise depths as would be indicated for continuous schemes.

B. REAL CASES

Ice thicknesses, surface heat losses to the atmosphere, and depths of penetration of surface-freezing induced convective overturn are treated in an analogous manner. Additionally however, ice thickness and mean surface heat-loss densities are presented as functions of time for run number 13, in which the model was integrated to represent 30 days of lead reclosure. Values for surface ice thicknesses were determined analogously to those of 48-hour ice-growth rates.

Table III. Ice Growth Rates, Test Cases.

Maximum Ice Thickness (cm) Occurring on the Lead's Surface at Eight-Hour Intervals.

Run Number	Time After Lead Generation						
	0	8	16	24	32	40	48
1	0	7.41	11.4	14.1	16.1	17.8	19.3
2	0	7.62	11.8	14.6	16.8	18.7	20.3
3	0	8.11	12.6	15.8	18.5	20.7	22.8
4	0	8.23	13.0	16.4	19.2	21.7	23.9
5	0	7.43	11.5	14.1	16.2	18.0	19.5
6	0	7.10	11.3	14.0	16.1	17.8	19.4
7	0	8.13	12.7	15.9	18.6	20.9	23.0
8	0	8.14	12.3	15.8	18.6	21.2	23.5

Figure 5. Ice Growth Rates, Test-Case Runs 1 - 4.

*from Table III

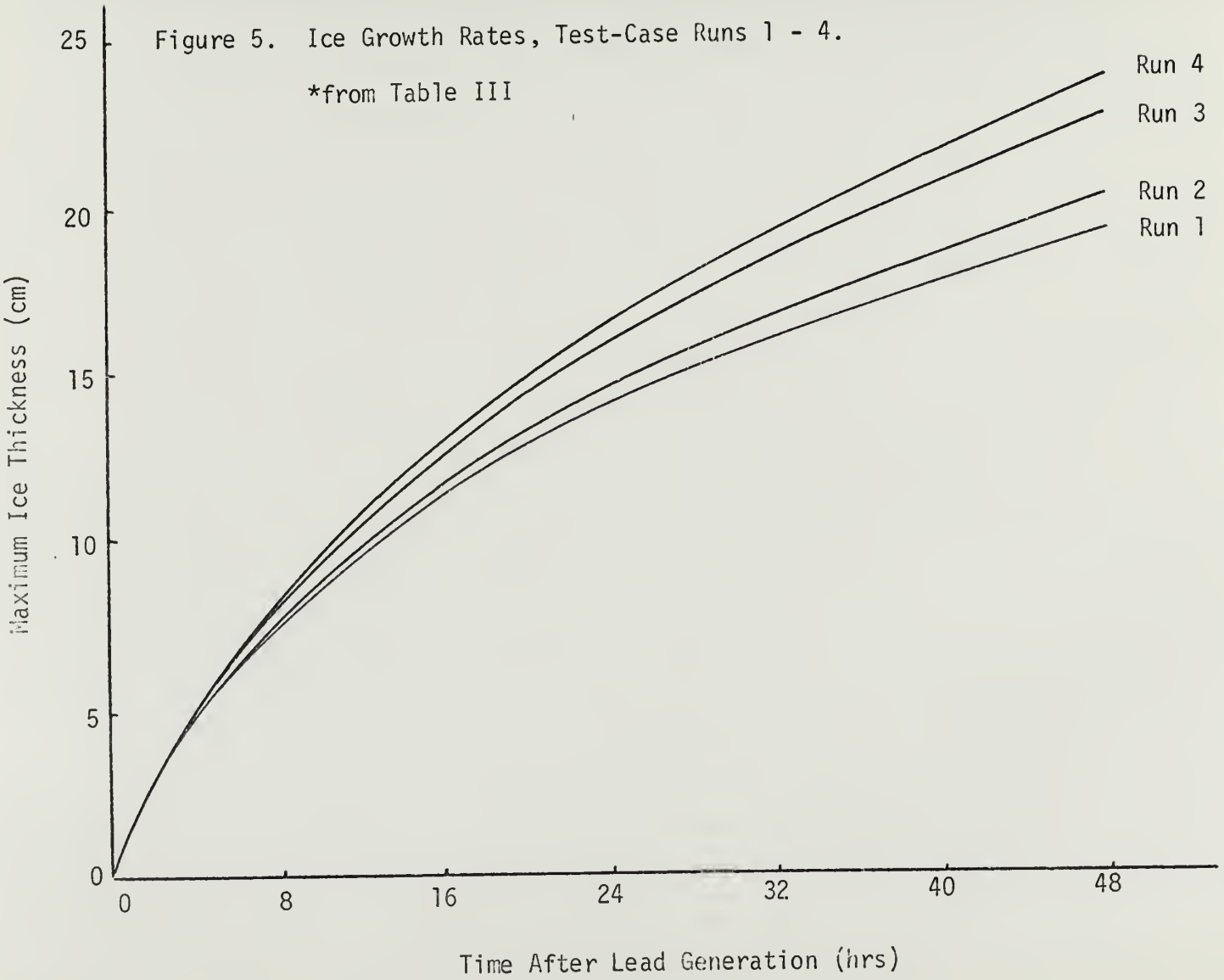

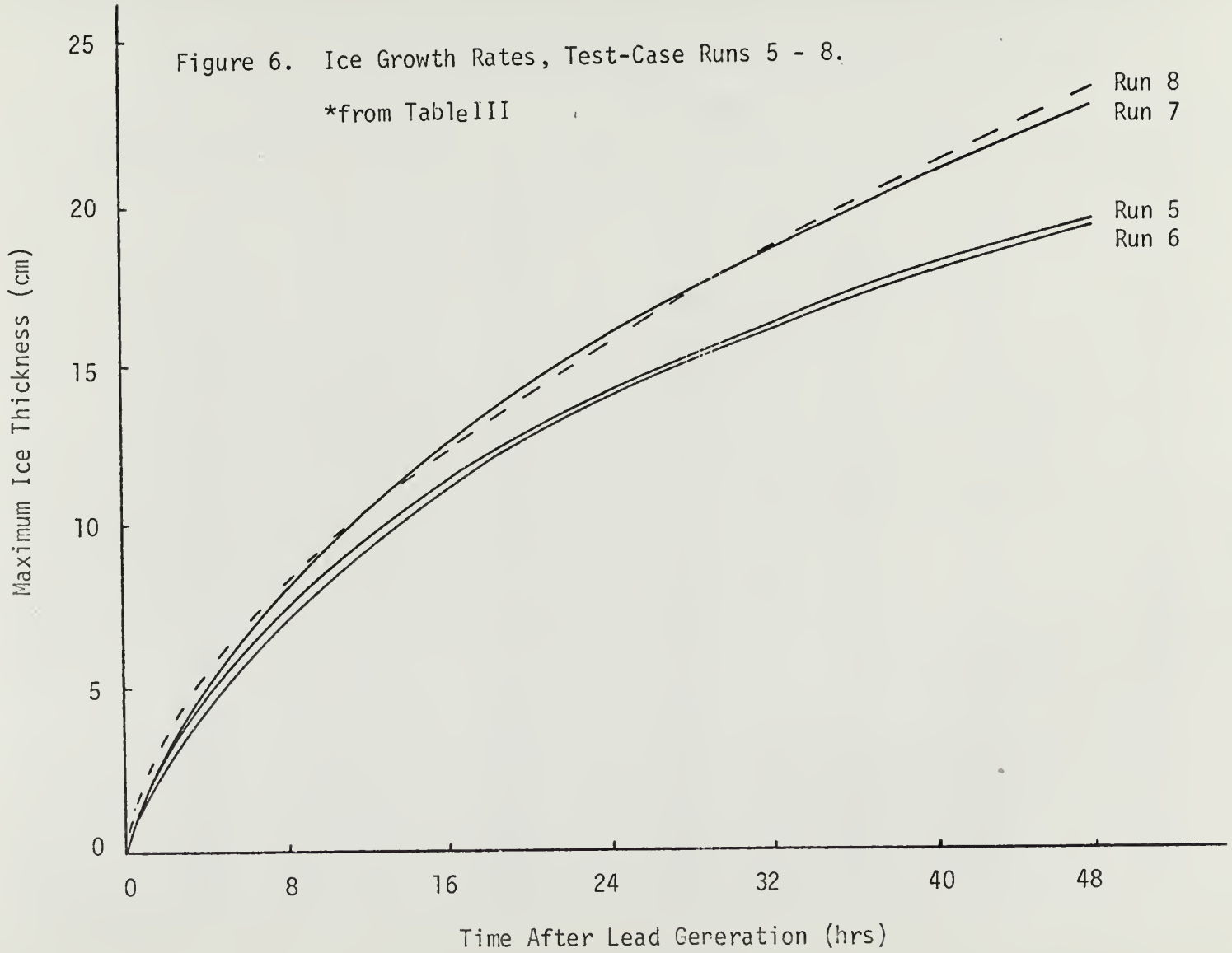

Figure 6. Ice Growth Rates, Test-Case Runs 5 - 8.

*from TableIII

Table IV. Ice Thickness Profiles, Test Cases.

Ice Thicknesses (cm) Across Lead Surface 48 Hours After Lead Generation

X (m)	Run Number							
	1	2	3	4	5	6	7	8
10	19.3	20.3	22.8	23.9	19.3	0.00	22.8	23.1
20	19.3	20.3	22.8	23.9	19.3	8.10	22.8	21.8
30	19.3	20.3	22.7	23.9	19.3	19.3	22.8	16.1
40	19.3	20.3	22.8	23.9	19.3	19.4	22.8	22.1
50	19.3	20.3	22.8	23.9	19.4	17.3	22.8	23.5
60	19.3	20.3	22.8	23.9	19.4	14.3	22.9	23.5
70	19.3	20.3	22.8	23.9	19.4	9.24	22.9	22.0
80	19.3	20.0	22.8	23.5	19.4	0.00	22.9	22.2
90	19.3	19.1	22.8	22.4	19.4	8.34	22.9	21.9
100	19.3	18.8	22.8	22.1	19.4	10.5	22.9	20.9
110	19.3	18.5	22.8	21.6	19.4	15.9	22.9	21.1
120	19.3	17.9	22.8	21.7	19.5	16.0	22.9	20.7
130	19.3	17.3	22.8	21.4	19.5	15.3	23.0	22.8
140	19.3	16.7	22.8	21.2	19.5	13.9	23.0	23.2
150	195.	94.4	200.	198.	195.	197.	201.	202.
160	195.	198.	200.	200.	195.	201.	201.	203.
170	195.	198.	200.	201.	195.	201.	201.	203.
180	195.	198.	200.	202.	195.	201.	201.	203.
190	195.	198.	200.	202.	195.	201.	201.	203.
200	195.	198.	200.	202.	195.	201.	201.	203.

Figure 7. Ice Thickness Profiles, Test-Case Runs 1 - 4.

* from Table IV

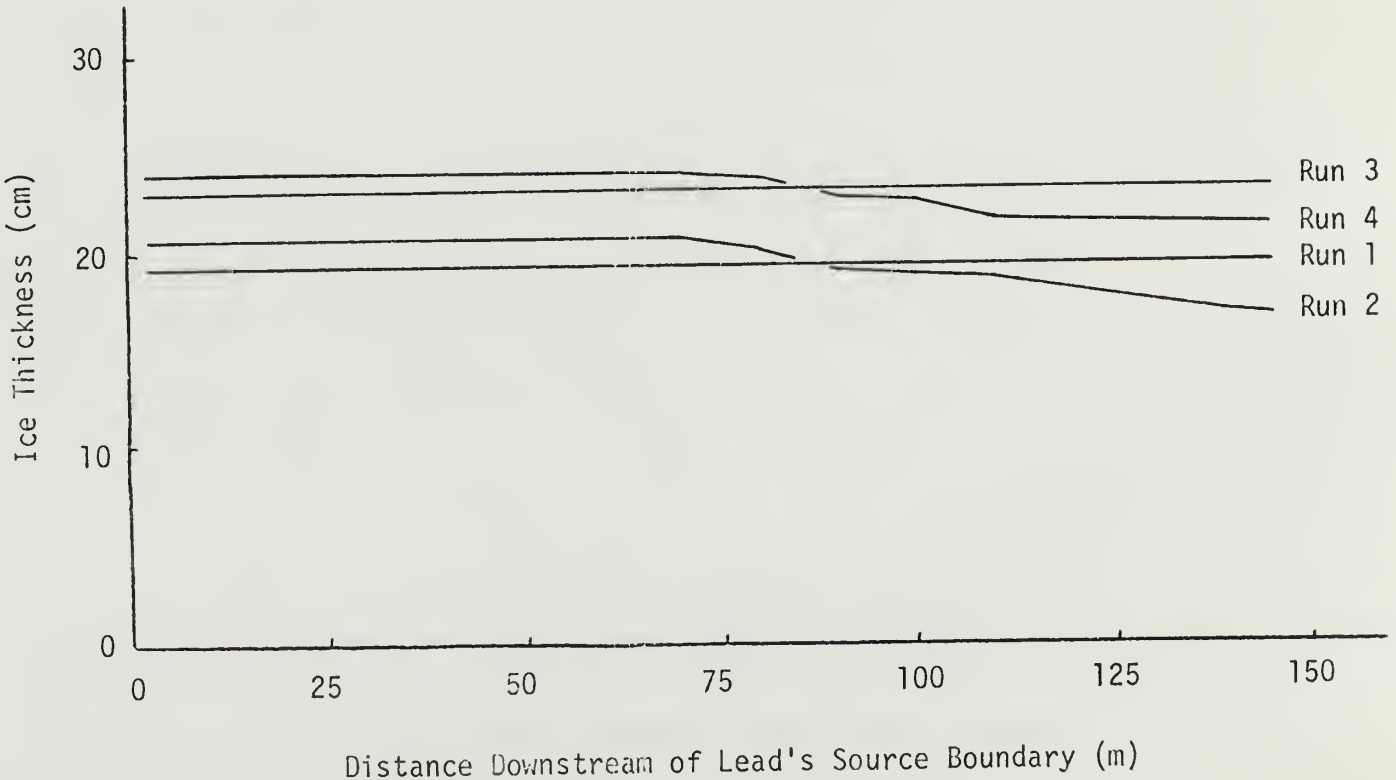

Figure 8. Ice Thickness Profiles, Test-Case Runs 5 - 8.

* from Table IV

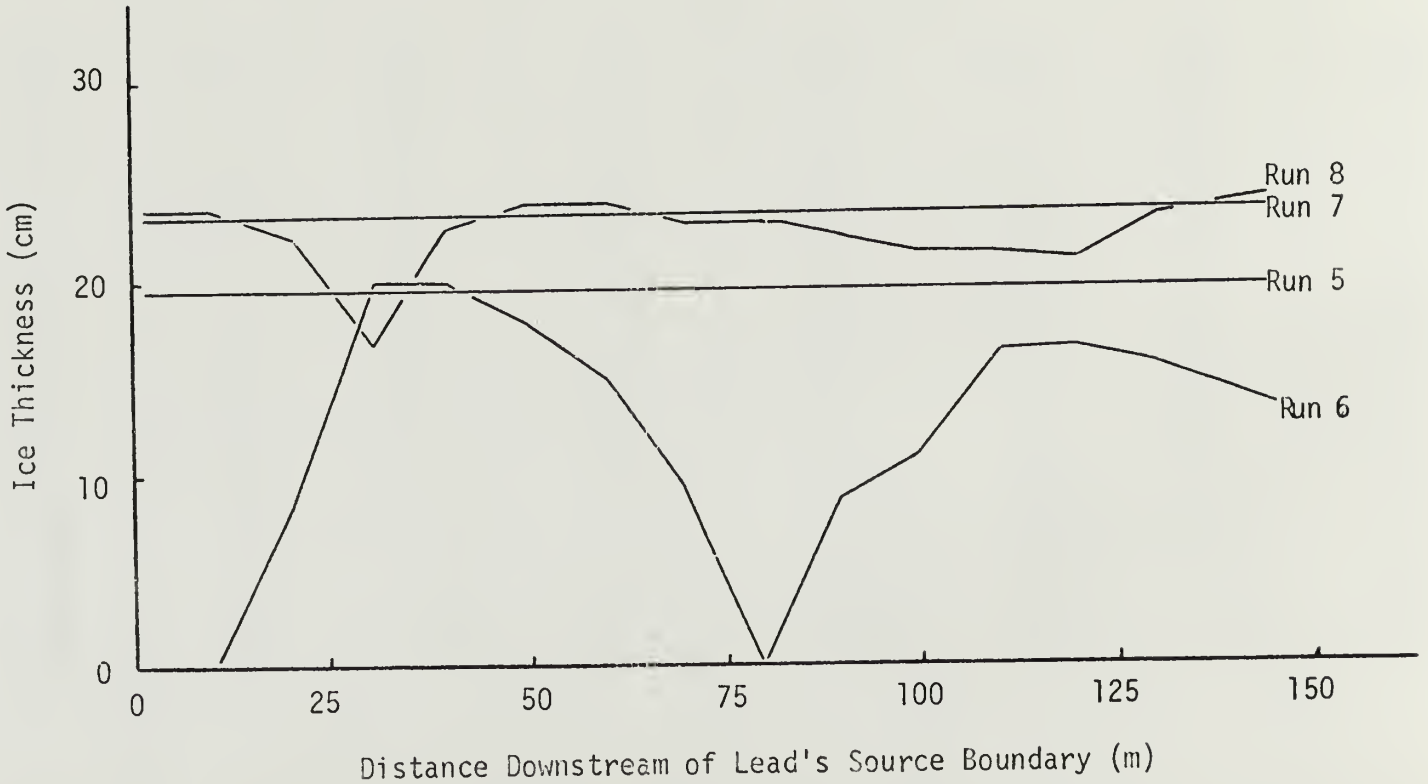

Table V. Surface Heat-Loss Densities, Test Cases

48-Hour Surface Heat Losses (x 10^2 cal/cm^2)

X (m)	Run Number							
	1	2	3	4	5	6	7	8
10	14.9	14.5	13.7	13.4	14.9	34.5	13.7	14.7
20	14.9	14.5	13.7	13.4	14.9	24.1	13.7	14.8
30	14.9	14.5	13.7	13.4	14.9	15.1	13.7	15.2
40	14.9	14.5	13.7	13.4	14.9	17.6	13.7	14.7
50	14.9	14.5	13.7	13.4	14.9	22.5	13.7	13.9
60	14.9	14.5	13.7	13.4	14.9	27.2	13.7	13.9
70	14.9	14.5	13.7	13.4	14.9	29.5	13.7	15.4
80	14.9	15.4	13.7	14.1	14.9	24.1	13.7	14.6
90	14.9	17.7	13.7	16.4	14.9	17.2	13.7	14.2
100	14.9	18.4	13.7	17.0	14.9	20.1	13.7	14.2
110	14.9	19.3	13.7	17.4	14.9	21.0	13.7	14.2
120	14.9	20.5	13.7	16.7	14.9	23.1	13.7	14.7
130	14.9	21.8	13.7	16.6	14.9	24.2	13.7	14.3
140	14.9	23.2	13.7	16.3	14.9	25.2	13.7	14.1
150	1.98	2.62	1.97	1.98	1.98	1.98	1.97	1.96
160	1.98	1.97	1.97	1.97	1.98	1.97	1.97	1.96
170	1.98	1.97	1.97	1.97	1.98	1.97	1.97	1.96
180	1.98	1.97	1.97	1.97	1.98	1.97	1.97	1.96
190	1.98	1.97	1.97	1.97	1.98	1.97	1.97	1.96
200	1.98	1.97	1.97	1.96	1.98	1.97	1.97	1.96

Figure 9. Surface Heat-Loss Densities, Test-Case Runs 1 - 4.

* from Table V

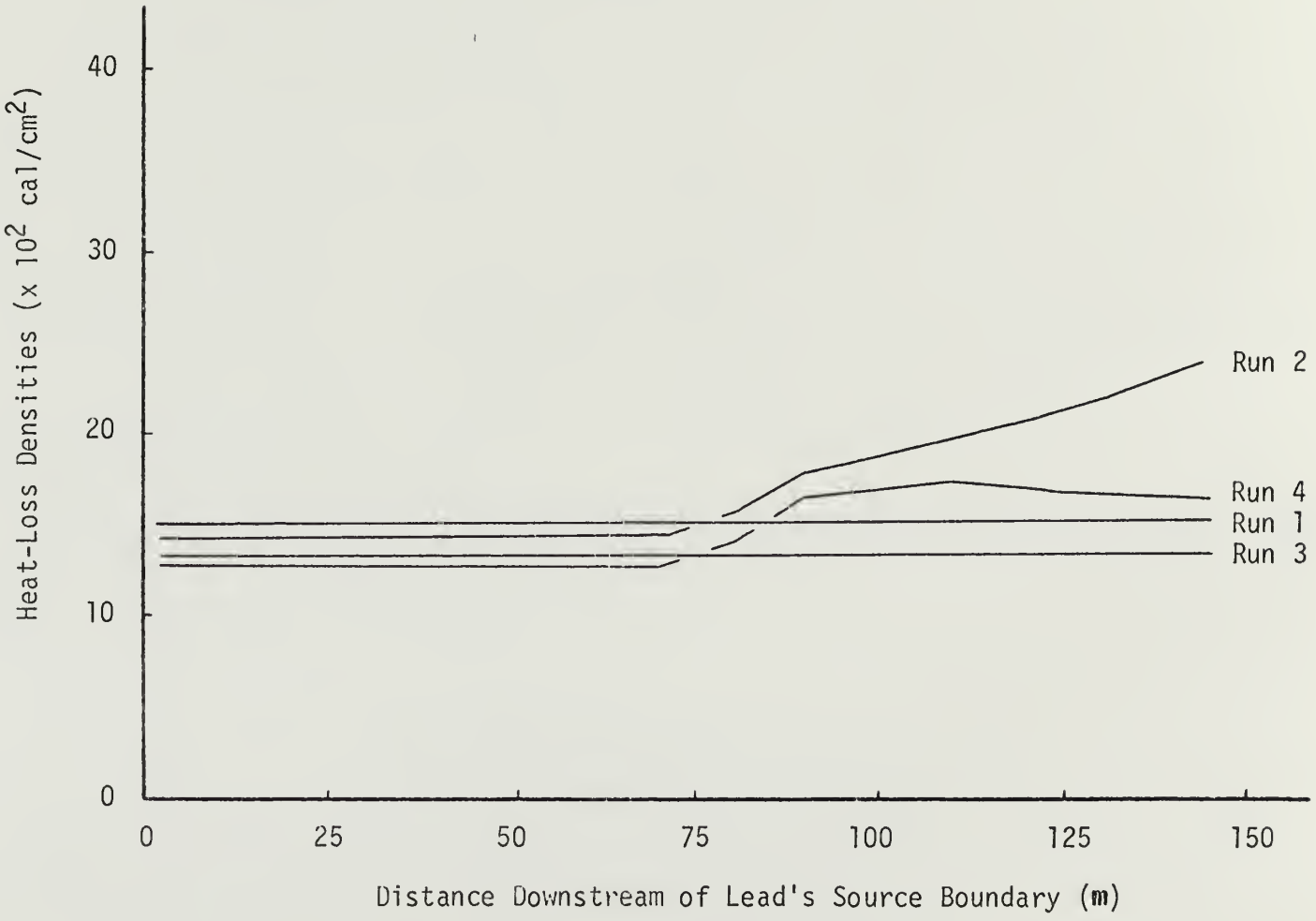

Figure 10. Surface Heat-Loss Densities, Test-Case Runs 5 - 8.

* from Table V

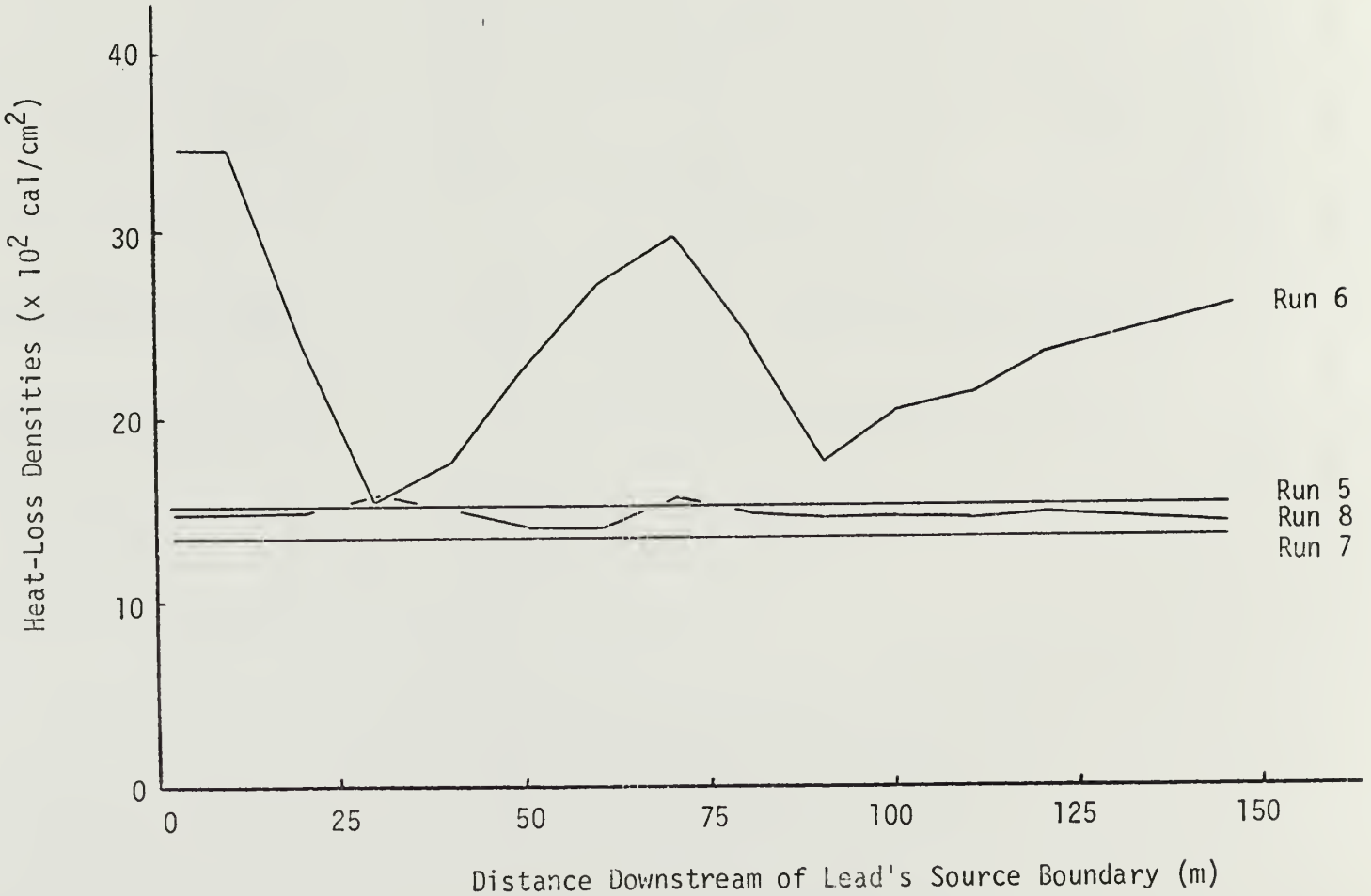

Table VI. Mean Surface Heat-Loss Densities, Test Cases.

48-Hour Mean-Surface Heat Losses
($\times 10^2$ cal/cm^2)

Run Number	$\overline{\Delta Q}$
1	14.9
2	17.0
3	13.7
4	14.9
5	14.9
6	23.2
7	13.7
8	14.5

Table VII. Maximum Depth of Penetration of Convective Overturn, Test Cases.

Run Number	Depth (m)
1	5
2	10
3	5
4	10
5	5
6	20
7	5
8	20

Table VIII. Ice Growth Rates, Real Cases.

Maximum Ice Thickness (cm) Occurring on the Lead's Surface at Eight-Hour Intervals.

Run Number	Time After Lead Generation						
	0	8	16	24	32	40	48
11	0	8.34	13.2	16.7	19.7	22.3	24.7
12	0	8.21	13.1	16.6	19.6	22.2	24.6

Figure 11. Ice Growth Rates, Real Cases.

* from Table VIII

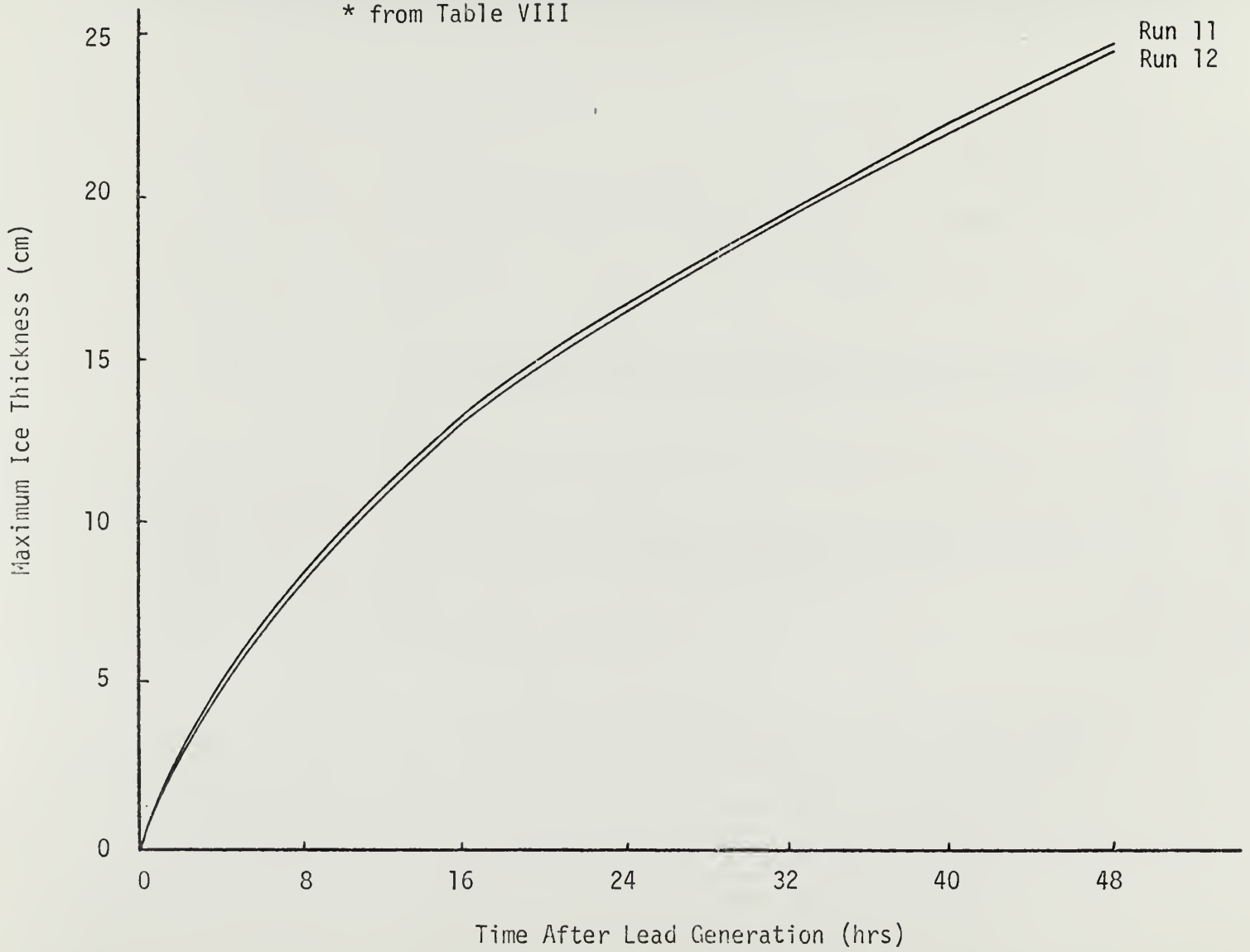

Table IX. Ice Thickness Profiles, Real Cases.

Ice Thicknesses (cm) Across Lead Surface
48 Hours After Lead Generation.

X (m)	Run Number	
	11	12
10	24.7	24.6
20	24.7	24.6
30	24.7	24.6
40	24.7	24.6
50	24.6	24.3
60	24.3	24.0
70	24.4	24.2
80	24.4	24.2
90	24.4	24.1
100	24.4	23.9
110	24.3	23.9
120	24.2	23.6
130	24.0	23.5
140	24.0	23.4
150	203.	203.
160	203.	203.
170	203.	203.
180	203.	203.
190	203.	203.
200	203.	203.

Figure 12. Ice Thickness Profiles, Real Cases

* from Table IX

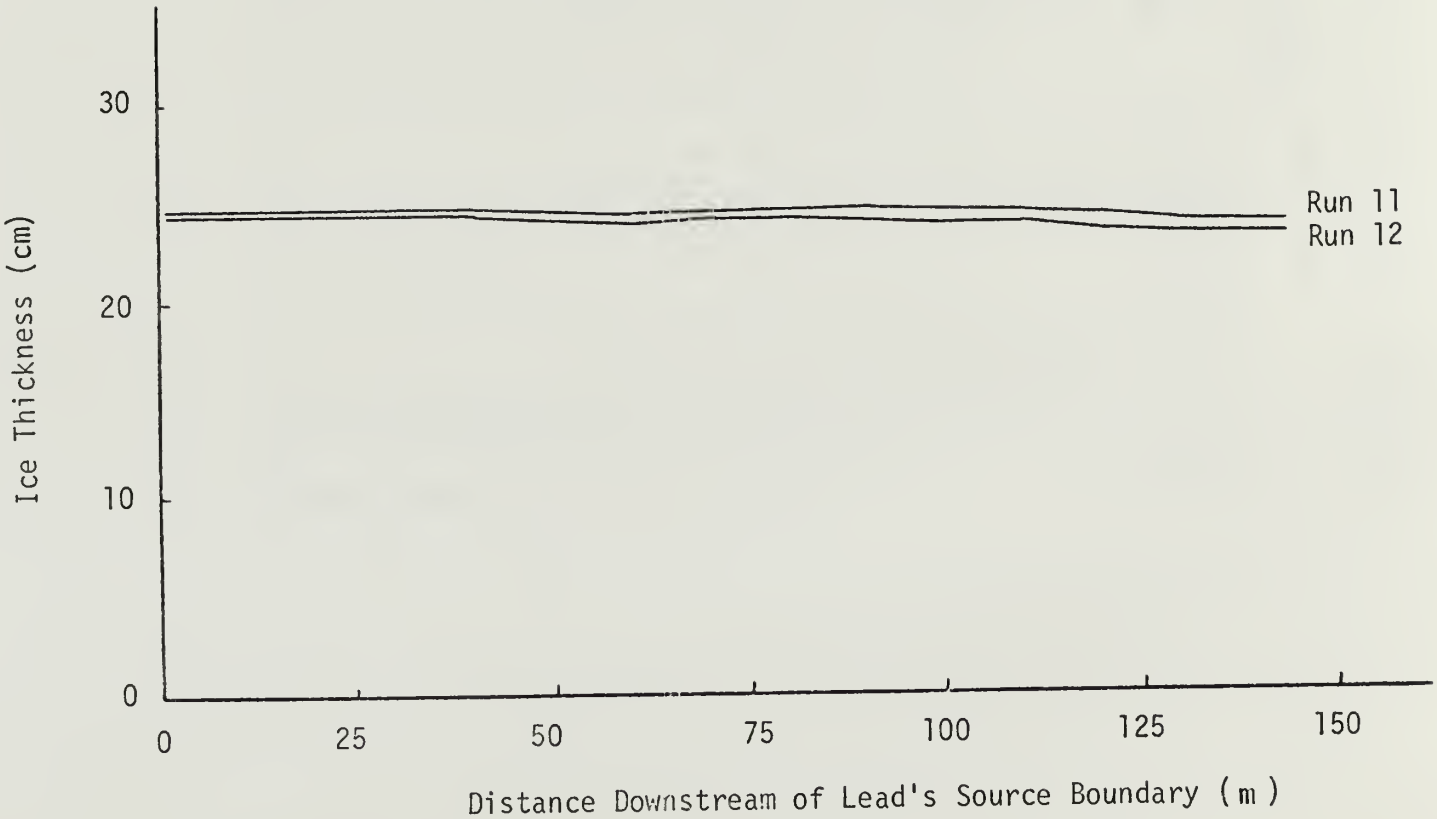

Table X. Surface Heat-Loss Densities, Real Cases.

48-Hour Surface Heat Losses
($\times 10^2$ cal/cm^2)

X (m)	Run Number	
	11	12
10	13.6	13.9
20	13.6	13.9
30	13.6	13.9
40	13.6	13.9
50	13.7	14.3
60	14.2	14.7
70	14.0	14.4
80	13.9	14.3
90	13.8	14.3
100	13.8	14.3
110	13.8	14.3
120	13.8	14.3
130	13.8	14.3
140	13.8	14.2
150	1.99	2.01
160	1.99	2.01
170	1.99	2.01
180	1.99	2.01
190	1.99	2.01
200	1.99	2.01

Figure 13. Surface Heat-Loss Densities, Real Cases.

* from Table X

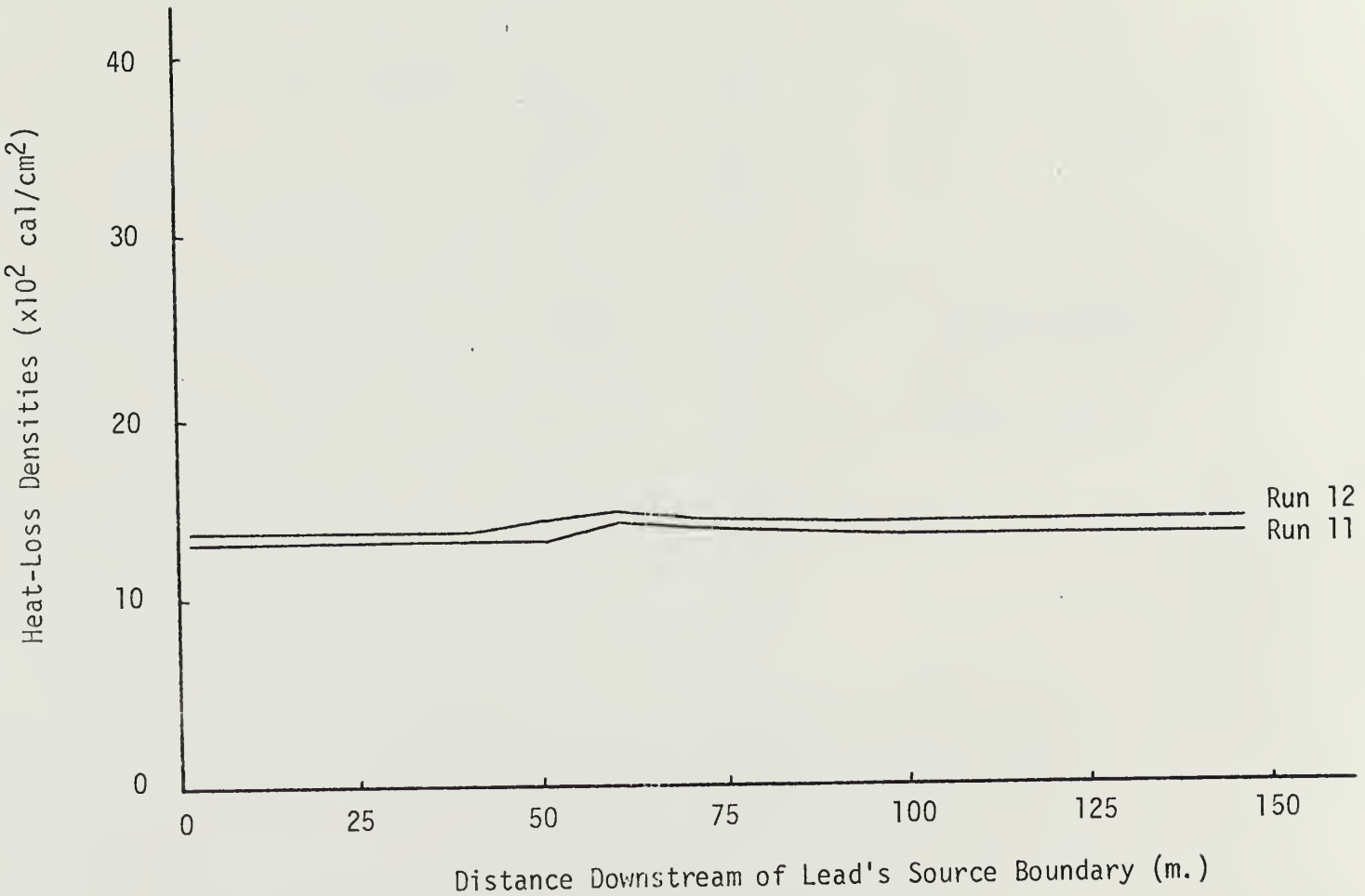

Table XI. Mean Surface Heat-Loss Densities, Real Cases.

48-Hour Mean Surface Heat Losses (x 10^2 cal/cm^2)

Run Number	$\overline{\Delta Q}$
11	13.8
12	14.2

Table XII. Maximum Depth of Penetration of Convective Overturn, Real Cases.

Run Number	Depth (m.)
11	15
12	15

Table XIII. Ice Growth Rate, Run 13.

Maximum Ice Thickness (cm) Occurring in the Lead's Surface at Five-Day Intervals.

Day	Ice Thickness
5	40.6
10	59.6
15	74.9
20	88.3
25	101.
30	112.

Table XIV. Mean Surface Heat-Loss Densities, Run 13.

Mean Surface Heat-Loss Densities ($x10^2$ cal/cm^2) at Five-Day Intervals.

Day	$\overline{\Delta Q}$
5	23.5
10	34.7
15	43.7
20	51.6
25	58.8
30	65.5

Figure 14. Ice Growth Rate, Run 13.

* from Table XIII

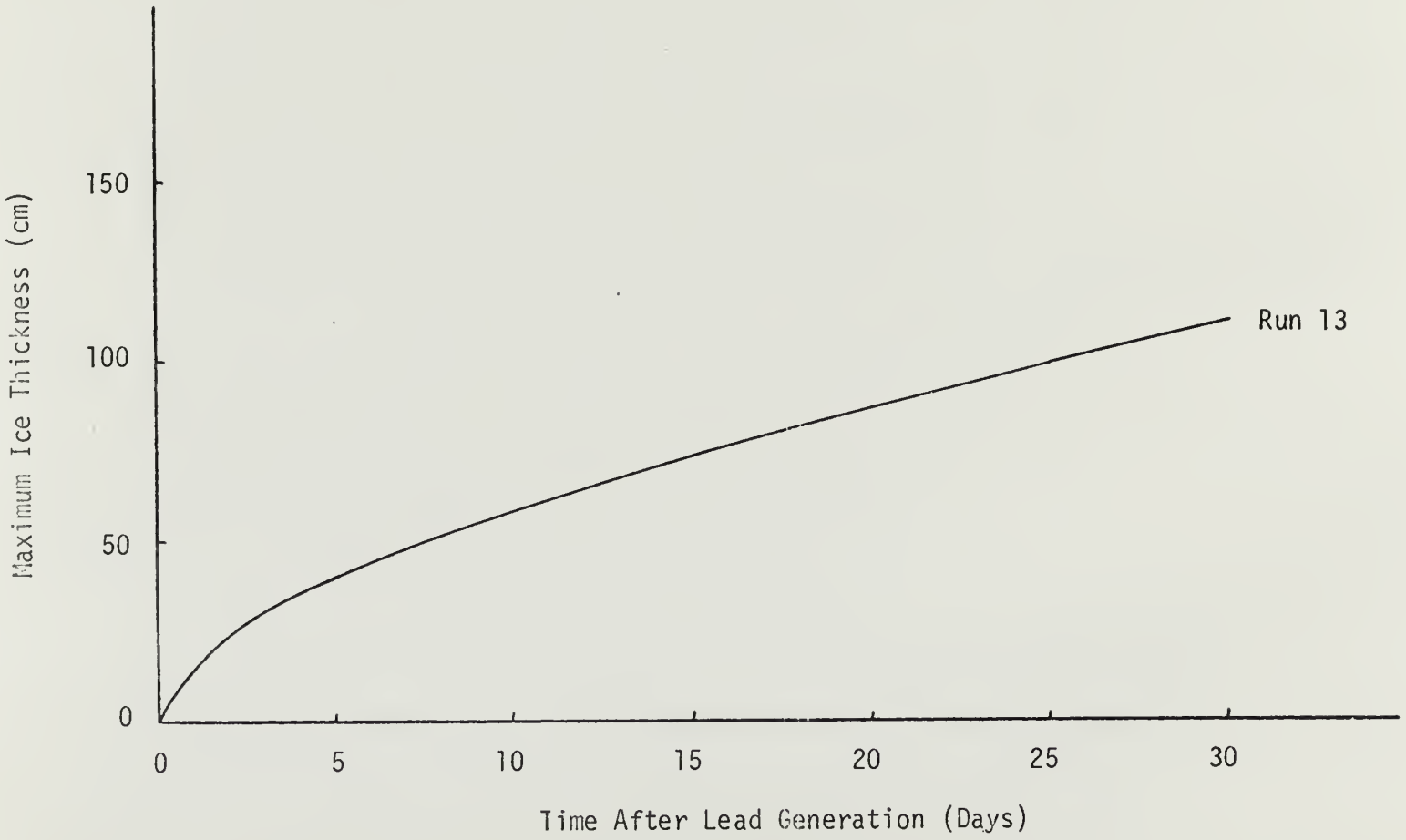

Figure 15. Mean Surface Heat-Loss Densities, Run 13.

* from Table XIV

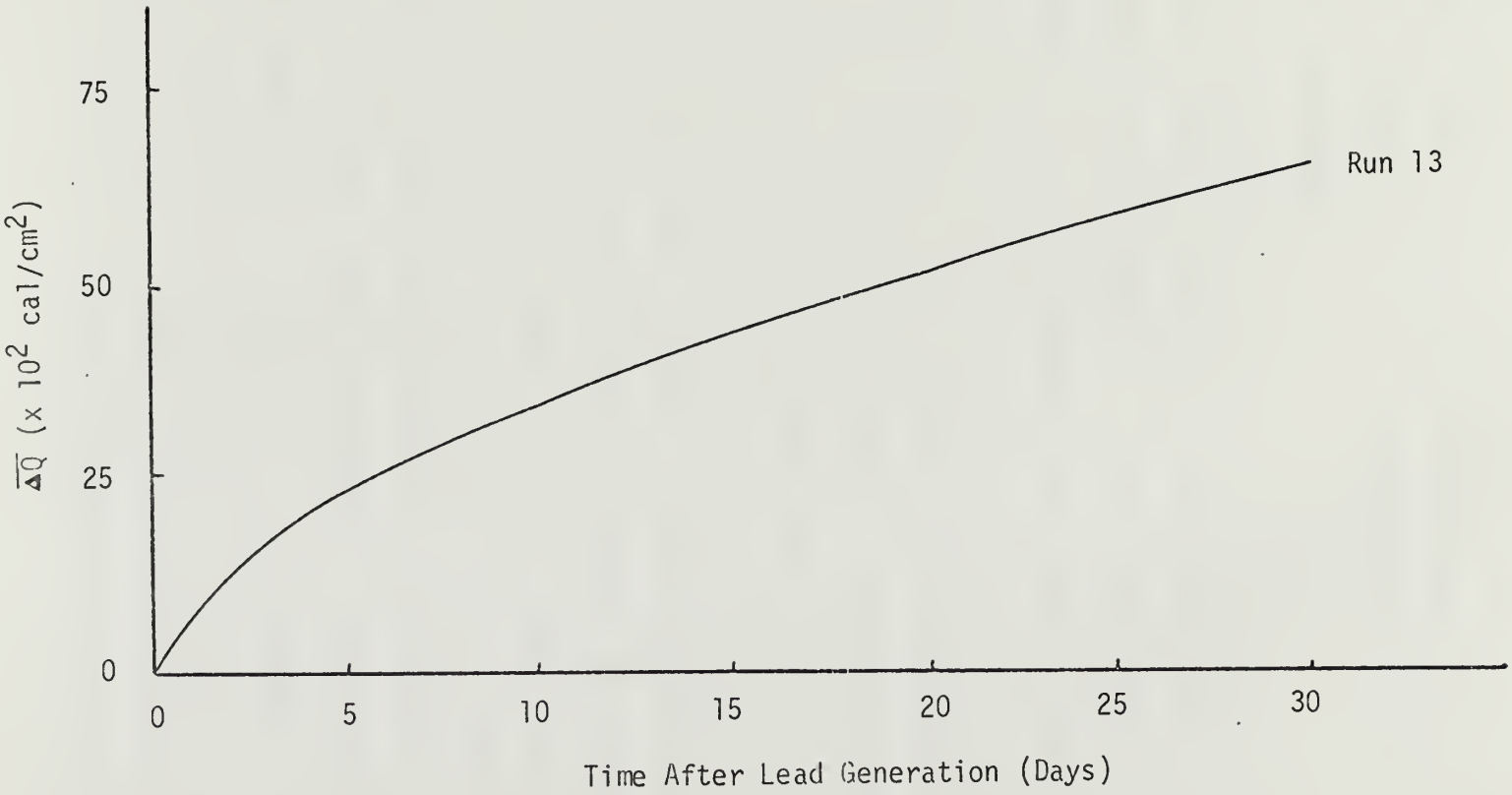

V. CONCLUSIONS

Through the preceding data and the time-dependent temperature-salinity-density fields generated in the lead model, numerous insights to the process of lead reclosure were afforded, as well as to the hydrodynamic validity of the model under certain conditions.

Perhaps most pronounced was the very strong role played by the near-surface vertical salinity gradient in maintaining water-column stability. A strong halocline near the surface tended to insulate deeper waters in the lead from the thermodynamic activity occurring at the surface. Surface waters whose densities had been increased by salt rejected by newly forming ice, was not able to mix vertically until density instabilities occurred in the surface region, thus inducing convective overturn. Since the presence of a strong surface halocline would require higher surface-salinity accumulations and hence permit more ice formation and associated salt rejection before this surface layer would become unstable, a strong halocline would be expected to inhibit convective overturn, both in frequency of occurrence and depth of penetration in the lead. Added to this insulating effect is the fact that, as surface salinities increase, surface freezing temperatures correspondingly decrease such that freezing rates are proportionately lowered.

The role played by the vertical temperature gradient in lead thermodynamics was strongly dependent upon the existing vertical salinity gradient. Since density changes in sea water at temperatures near the freezing point are almost totally a function of salinity changes, the insulating qualities of the thermocline are undefinable when treated independently of the halocline.

However, in situations wherein weak vertical salinity gradients (poor insulation) and strong vertical temperature gradients coexisted, convective overturn resulted in relatively large quantities of heat being transported to the surface. Freezing and associated salt rejection were thus inhibited and surface melting was induced. In this manner, the temperature stratification was superimposed on the primary control exerted by the vertical salinity gradient.

The effect of horizontal current magnitude on lead stability appeared, as in the case of the thermocline, to be secondary to the effect of the halocline. Strong currents will advect surface salt accumulations out of the lead relatively quickly, and will in general allow less time for lead thermodynamics to affect a given parcel of water advectively transiting the lead's width. This allows less change in the parcel's physical characteristics. Through these effects, the current also acts as an insulating agent.

Ice growth rates were clearly dependent upon combinations of the above three variable parameters. Neglecting spacial ice profiles across the lead temporarily and examining only the maximum ice thicknesses occurring on the lead's surface as a function of time, the highest growth rates were exhibited for cases where a strong current, a weak thermocline, and a weak halocline occurred together. Conversely, lowest growth rates resulted from the coexistence of a strong current, a strong thermocline, and a strong halocline. Very little difference however, was noted in the high growth-rate case when currents were weak instead of strong, nor in the low growth-rate case when currents were weak or when currents were weak and the halocline was weak. Analysis of these results showed that high growth rates were in all cases associated with weak vertical temperature gradients and low growth rates with strong vertical temperature gradients. Further, that current

strength was relatively unimportant in changing growth rates when either strong haloclines were present, or when weak temperature gradients together with weak salinity gradients were present.

The effect of the near-surface vertical temperature gradient appears then to dominate in determining surface freezing rates. Strong gradients resulted in lower rates of ice formation than in the case of weak gradients. Vertical transport of heat from depth in the lead by both eddy diffusion and convective overturn is then modified by both current strength and the near-surface halocline acting as insulating agents.

Ice thickness profiles across the lead's width varied considerably with different combinations of the three basic variable parameters. Uniform or nearly-uniform ice thicknesses across the lead were in all cases associated with strong near-surface haloclines. Variations occurred where weak haloclines existed, growing larger when weak haloclines and strong thermoclines occurred together. The greatest surface irregularity, both by amplitude of variation as well as by spacial frequency of variation, was found when weak currents, weak haloclines, and strong thermoclines occurred together.

Analysis of these cases indicated that the halocline was the dominant variable in determining uniformity of ice thickness across the lead through insulation of the surface from the heat at depth in the lead. When convective overturn occurred as a result of increases in surface salinity, surface freezing rates were altered at the point of convective overturn and produced surface irregularities. Since rejected salt is being continuously advected downstream, there will exist horizontal salinity gradients which, when exceeding the magnitudes of vertical salinity gradients, will induce convective overturn and resultant surface melting at that point. Downstream of this point,

surface waters are diluted due to the upstream melting, thus experiencing increased freezing rates since their freezing point has effectively been raised.

The near surface thermocline appeared to affect surface-ice uniformity through determining the amount of heat transported to the surface during convective overturn, and thus the amount of melting and dilution occurring. Finally, current strength appeared to act analogously to the halocline as an insulating agent, though less effectively. By flushing surface-salt accumulations out of the lead more rapidly, a strong current appears to inhibit convective overturn and hence variations in ice uniformity. By decreasing the amount of change a given parcel of water experiences over a given horizontal distance in the lead, a strong current appears to produce less intensive but more extensive lee effects from surface dynamics.

Surface heat-loss densities varied across the lead's surface in response to ice thickness profiles. Since open-water sensible, latent, and radiative heat-flux densities used in this work totalled 2.00×10^{-2} cal/cm^2-sec as compared to a corresponding value over the 200 cm of ice of 1.15×10^{-3} cal/cm^2-sec, resultant heat-loss densities were considerably larger over regions of the lead surface covered with relatively thinner ice. Uniformity of surface heat-loss densities over the lead's surface may then be directly related to the uniformity of the ice profile over the surface, while relative magnitudes of heat-loss densities may be inversely related to relative ice thicknesses.

The extreme case of lead instability and non-uniformity (weak current, strong thermocline, and weak halocline) requires special comment. A high mean surface heat-loss density characterized this case, which was expected as a result of its highly non-uniform surface-ice profile. However, the lack

of evidence of these highly non-uniform ice covers occurring in nature in the absence of mechanical deformation forces prompted further analysis. By studying model output fields of runs 2, 6, 9, 10, and 14 (particularly the horizontal density gradients generated in the lead), an upstream pressure force was found to exist in the vicinity of the source boundary which was capable of performing on the order of ten ergs of work against a unit mass of water entering the lead at the source boundary. Since a thermodynamically generated force of this type would completely alter the hydrodynamics occurring in the lead for low current magnitudes, the model appears to be non-representative of actual lead thermodynamics when using very low current magnitudes with strong thermoclines and weak haloclines. Stronger currents, on the other hand, had generally weaker horizontal density gradients associated with them and were also proportionately less affected by these pressure forces since their capacity to do work against the horizontal pressure force increases as the square of their magnitude.

Results of run 14 proved to be of particular interest through the insights they afforded to the process of convective overturn. Since no current was present, there was no horizontal coupling between model grid points. As a result, although freezing progressed uniformly over the surface of the lead, strong differential horizontal density gradients developed along the 'source' boundary as cooling progressed. Of prime interest however, was the graphic illustration of the role played by the current as a convective-overturn scaling factor. With zero current, a strong temperature gradient and a weak salinity gradient, freezing-induced convective overturn penetrated to a depth of 35 meters roughly 18 hours after lead generation. Without the flushing action of a horizontal current or the insulating effect of a strong

halocline, the effects of surface thermodynamics were felt much deeper in the lead. It appears probable then, that in cases wherein weak currents and weak haloclines exist in open leads (marginal vertical stability), surface freezing will induce, through convective overturn and vertical mixing, substantial vertical and horizontal gradients in both temperature and salinity. As a result, significant fluxes of heat, salt, and momentum would be generated in the waters of the lead, and sophistication beyond that possessed by the work at hand would be required to accurately represent the resultant lead hydrodynamics.

Summarizing the analysis of results from integrating the open-lead model over the experimental ranges of variables, the near-surface vertical salinity gradient appears to exert the dominant force in maintaining vertical density stability in the water column through its insulating effect. By inhibiting convective overturn, a strong halocline was associated with horizontally-uniform ice thickness profiles and consequently uniform surface heat-flux densities. Current strength and the vertical temperature gradient appeared to be secondary as insulating agents.

The near-surface temperature gradient appeared to be the dominant variable in controlling the rate of ice formation since its strength directly influences the amount of heat transported to the ice-water boundary from depth by both eddy diffusion and convective overturn. In this case, the halocline and the current strength appeared secondary in their effects on the freezing rate.

Mean surface heat-loss densities were higher for more non-uniform surface ice thicknesses, which in turn may be inversely related to the strength of the near-surface halocline. This conclusion could prove to be

of significance to critical examinations of the heat budget over large areas of the arctic in which significant regional variations in the near-surface halocline might reasonably be expected.

Representative freezing rates, ice-thickness profiles, and surface heat-loss densities found in integrating the model using real-case variables agreed well with values in the literature. Due to the similarity of current strengths, near-surface thermoclines, and near-surface haloclines, the foregoing relations were generally not discernable, although the effect of downstream salt accumulation was noticed in slightly decreasing downstream ice thicknesses.

Finally, it is concluded that, with the exception of cases in which weak horizontal currents occur together with strong thermoclines and weak haloclines, the model presented herein provides an accurate physical representation of the thermodynamics occurring in an open lead in central arctic sea ice over the experimental range of variables.

VI. RECOMMENDATIONS FOR FURTHER RESEARCH

Although the surface boundary of the model could be considerably more sophisticated in its treatment of energy fluxes and transport processes, models already exist which have this sophistication, notably that of Maykut and Untersteiner [1969, 1971]. Coupling the model at hand to their model would therefore seem a more reasonable approach to refinement of the surface boundary in order to model air-ice-sea interactions and mass-energy balances.

The hydrodynamics occurring in a refreezing lead however, are still not accurately modelled, nor are they fully understood despite the insights afforded by the research performed. Extended development of this work would promote further conceptual understanding of these processes as well as provide a more physically-accurate model. Incorporation of accelerations resulting from thermodynamically-generated horizontal pressure gradients, as well as the coriolis acceleration, would considerably refine the model. Additional refinement would be gained by removing previously discussed limitations on: 1) the minimum vertical salinity gradient able to be accurately treated, and 2) the preclusion of downstream advection of warmer-then-freezing-point waters under an ice cover.

In summary then, further research could profitably be applied to the work at hand to further refine the hydrodynamic accuracy of the model, as well as to couple it to larger-scale models of air-ice-sea interactions and mass-energy balance predictive schemes.

APPENDIX A

COMPUTER PROGRAM DESCRIPTION

The computer program is written in FORTRAN IV and was used with the IBM 360/67 computer system at the W.R. Church Computer Center, Naval Postgraduate School. The program has been generalized such that sea water temperature and salinity profiles used as initial and left boundary fields are treated as input data. A design feature of the program allows the use of an internally variable time step to facilitate adjusting the model's temporal resolution. Additionally, the model allows variable grid spacing as well as variable lead dimensions, requiring changes only in the DIMENSION, COMMON and FORMAT statements. Although all currents used in the model were constant in time and space, the model allows use of both a depth-dependent and time-dependent horizontal current, again internally variable. With only minor modifications, the program could be easily extended to include a bottom-boundary heat and salt flux, more sophisticated treatment of air-sea interactions at the surface boundary, and feedback of accelerations, resulting from horizontal density gradients generated by lead thermodynamics, to the motion of water through the lead.

The program is divided into two basic sections: the main program and subroutine OVRTRN. The main program is further subdivided into seven parts: problem initialization, data input, computation of time-dependent temperature and salinity fields, ice-accretion/melting and salt rejection/dilution, with vertical stability check and computation of resultant heat flux densities, filling temperature and salinity arrays with resultant values, computation of applied surface heat flux densities and conversion to an integrated surface

temperature gradient, and writing output. Subroutine OVRTRN accomplishes vertical convective overturn and mixing of unstable regions in the water column.

FORTRAN IV symbols for primary program parameters are defined below:

AH	Downstream-advected heat-flux density (cal/cm^2-sec)
AHF	Applied surface heat-flux density (cal/cm^2-sec)
BTC	Sea ice thermal conductivity constant ($cal\text{-}cm^2/g\text{-}sec$)
CAH	Cumulative downstream-advected heat density (cal/cm^2)
CAHF	Cumulative applied surface heat density (cal/cm^2)
CHC	Cumulative subsurface cooling heat density (cal/cm^2)
CHF	Cumulative applied surface heat density less cumulative downstream-advected heat density (cal/cm^2)
CHIF	Cumulative heat density of surface-ice formation (cal/cm^2)
CI	Thermal conductivity of sea ice ($cal/cm\text{-}sec\text{-}^oC$)
CL	Sea-water chlorinity (g/kg)
CO	Thermal conductivity of pure ice ($cal/cm\text{-}sec\text{-}^oC$)
CP	Specific heat of sea water ($cal/g\text{-}^oC$)
DI	Rate of surface ice formation (cm^3/cm^2-sec)
DSALT	Salt rejected per cm^3 of ice formed (g/kg)
DTAU	Time step (sec)
DTEMP	Air-water temperature difference (^oC)
DX	Horizontal grid spacing (cm)
DZ	Vertical grid spacing (cm)
EPS	Allowable rate-of-freezing error (cm^3/cm^2-sec)
ERR	Allowable ice thickness error (cm^3/cm^2)
GRADI	Vertical ice temperature gradient ($^oC/cm$)

H	Model depth extent (cm)
HC	Subsurface cooling heat-flux density (cal/cm^2-sec)
HF	Applied surface heat-flux density less downstream-advected heat flux density (cal/cm^2-sec)
HIF	Heat-flux density of surface-ice formation (cal/cm^2-sec)
HO	Heat of formation of pure ice (cal/g)
HS	Heat of formation of sea ice (cal/g)
MH1	Number of grid columns
MV1	Number of grid rows
MVH1	Total number of grid points
QI	Heat-flux density through sea ice to the atmosphere (cal/cm^2-sec)
QL	Open-water latent heat-flux density to the atmosphere (cal/cm^2-sec)
QR	Open-water radiative heat-flux density to the atmosphere (cal/cm^2-sec)
QS	Open-water sensible heat-flux density to the atmosphere (cal/cm^2-sec)
RHO	Density of sea water (g/cm^3)
RHOI	Density of sea ice (g/cm^3)
S	Sea-water salinity (g/kg)
SALI	Sea-ice salinity (g/kg)
SI	Sea-ice salinity (g/cm^3)
SIGT	Sigma-t
SSCHG	Salinity change in surface layer of depth DZ (g/kg)

SSFLUX	Salinity change in one cm^3 of sea water at the ice-water boundary (g/kg)
STGD	Total applied surface temperature gradient at the water's surface ($^oC/cm$)
T	Sea-water temperature (^oC)
Tau	Time (sec)
TF	Sea-water freezing temperature (^oC)
TGRADL	Surface temperature gradient due to latent heat-flux density ($^oC/cm$)
TGRADR	Surface temperature gradient due to radiative heat-flux density ($^oC/cm$)
TGRADS	Surface temperature gradient due to sensible heat-flux density ($^oC/cm$)
TI	Temperature of lower ice surface (^oC)
U	Horizontal current magnitude (cm/sec)
VEC	Vertical eddy conductivity (cal/cm-sec-^oC)
VSK	Vertical salt eddy diffusivity (cm^2/sec)
VTK	Vertical temperature eddy diffusivity (cm^2/sec)
W	Lead width (cm)
Z	Depth (cm)
ZI	Surface ice thickness (cm^3/cm^2)

A descriptive flow diagram of the program is shown in Figure 16.

Figure 16. Descriptive Flow Diagram of Program.

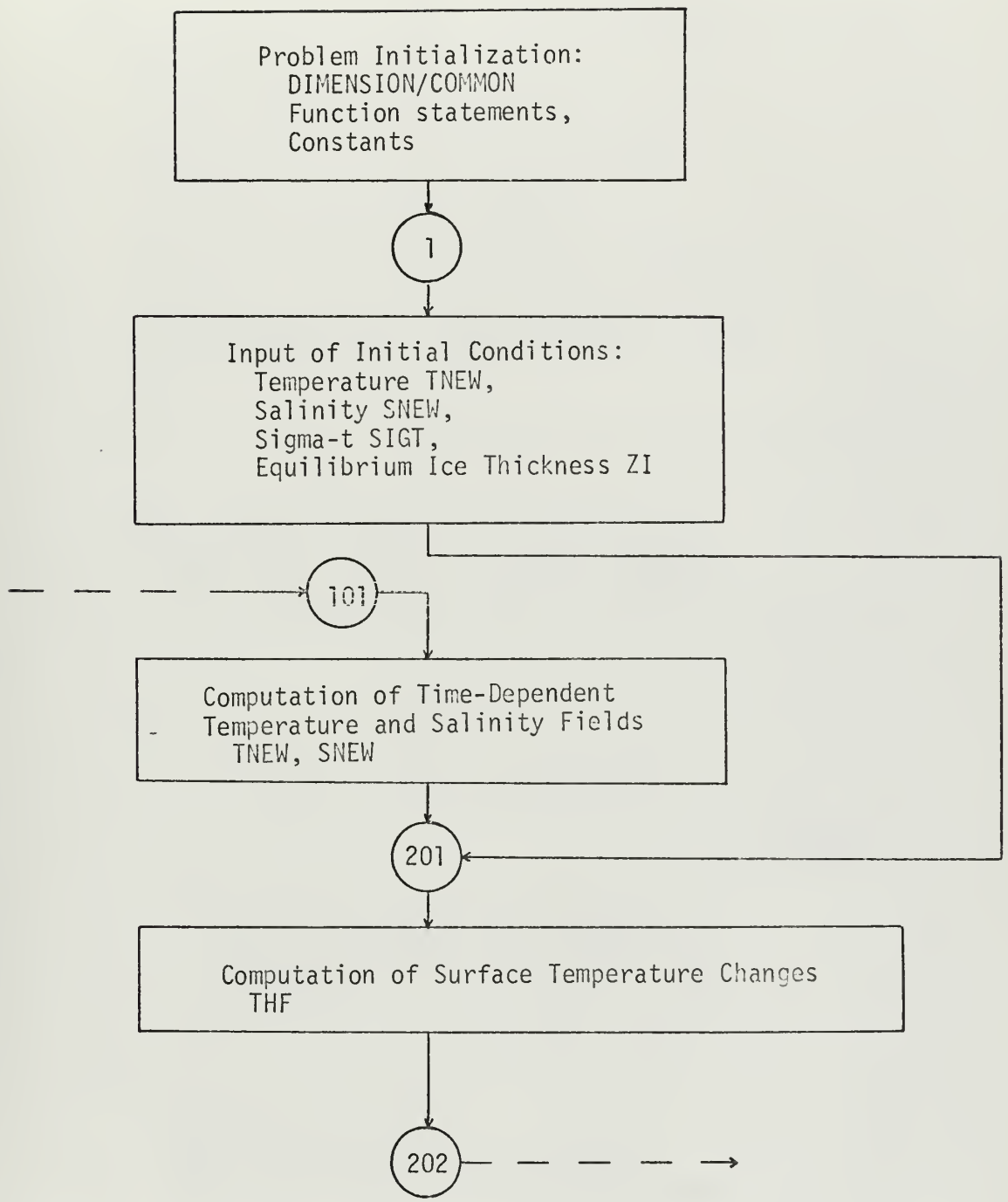

Figure 16 (continued).

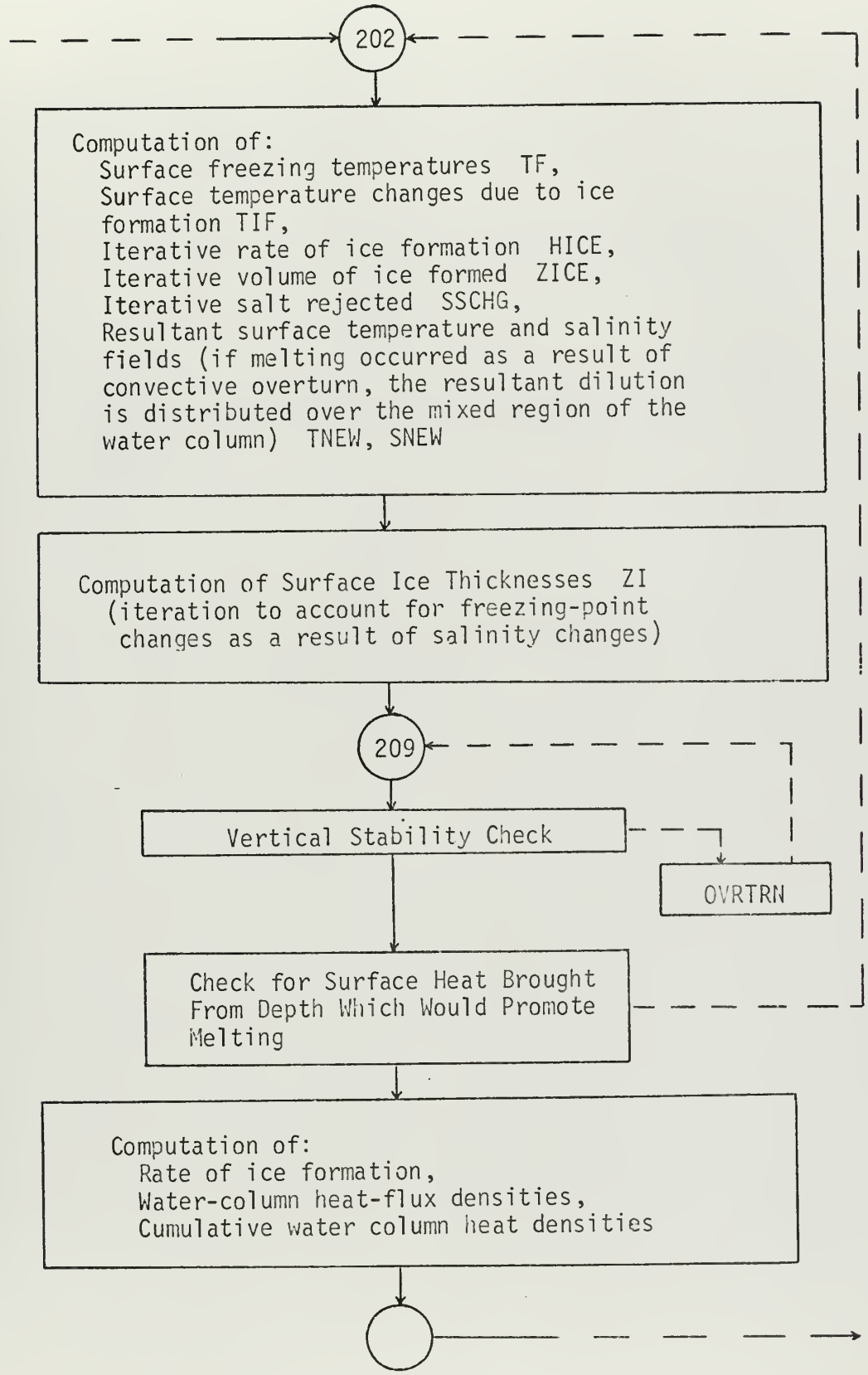

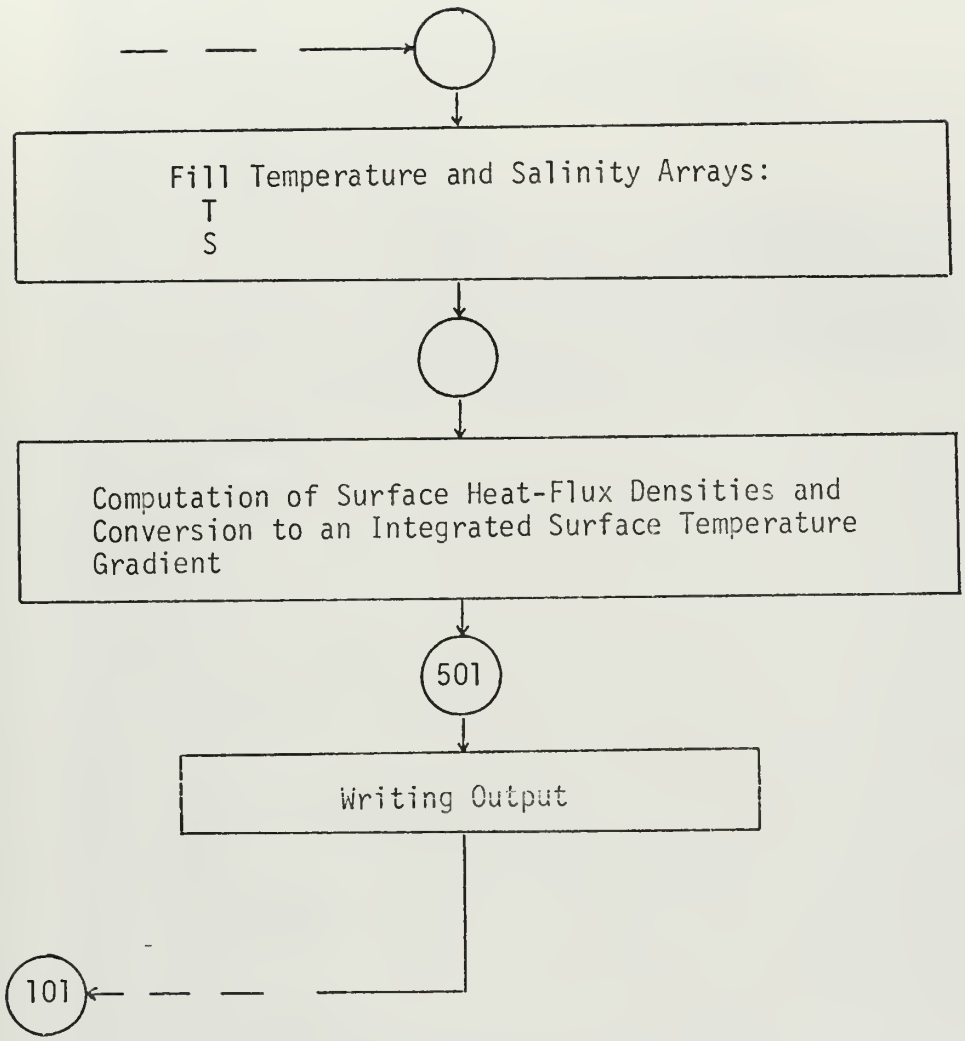
Fill Temperature and Salinity Arrays:
T
S
Computation of Surface Heat-Flux Densities and Conversion to an Integrated Surface Temperature Gradient
501
Writing Output
101

```
CENTRAL ARCTIC OPEN-LEAD MODEL.
      DIMENSION T(232),S(232),PUF(22),AH(22),CAH(22),
     1HIF(22),CHIF(22),DI(22),ZI(22),TF(22),HF(22),CHF(22),
     2STGD(22),HC(22),CHC(22),AHF(22),CAHF(22),HUF(22)
      COMMON TNEW(232),SNEW(232),SIGT(232)
      U(B)=7.0
      AT1(B)=1.-DTAU*(U(B)/DX+2.*VTK/DZ**2)
      AS1(B)=1.-DTAU*(U(B)/DX+2.*VSK/DZ**2)
      AT2(B)=DTAU*U(B)/DX
      AS2(B)=DTAU*U(B)/DX
      AT3(D)=D*VTK/DZ**2
      AS3(D)=D*VSK/DZ**2
      C(A)=(A-0.03C)/1.8050
      SO(A)=-0.069+1.4708*A-0.001570*A**2+0.0000398*A**3
      AT(A)=A*(4.7807-0.098185*A+0.0010843*A**2)*0.001
      BT(A)=A*(18.030-0.8164*A+0.01667*A**2)*0.000001
      ST(A)=-(A-3.98)**2/503.570*(A+283.)/(A+67.26)
      SGT(A)=A+(SIGO+0.1324)*(1.0-ATMP+(BTMP*(SIGO-0.1324)))
      SH(A)=1.005-0.004136*A+C.0001098*A**2-0.000001324*A**3
      DE(A)=1.0+(A/1000.)
      F(A)=0.0-(0.0966*A+0.0000052*A**3)
      R(C)=DSALT*C
      ERR(D)=D*EPS
      BTC=0.28
      CO=0.00486
      DTAU=90.0
      DTEMP=25.
      DX=1000.0
      DZ=500.0
      EPS=1.0E-8
      H=5000.0
      HO=79.77
      QL=3.0E-3
      QR=2.0E-3
      QS=1.5E-2
      RHOI=0.91
      SALI=8.0
      SI=RHOI*SALI/1000.0
      VSK=10.0
      VTK=10.0
      W=20000.0
      MH=IFIX(W/DX)
      MV=IFIX(H/DZ)
      MV1=MV+1
      MH1=MH+1
      MVH1=MV1*MH1
    1 READ(5,100)IRUN
      IF(IRUN.EQ.99)GO TO 1000
      READ(5,150)(TNEW(I),I=1,MV1)
      READ(5,150)(SNEW(I),I=1,MV1)
      CL=C(SNEW(1))
      TF(1)=F(CL)
      TNEW(1)=TF(1)
      M=MV1
      DO 3 J=2,MH1
      DO 2 K=1,MV1
      I=M+K
      TNEW(I)=TNEW(K)
      T(I)=TNEW(K)
      SNEW(I)=SNEW(K)
      S(I)=SNEW(K)
    2 CONTINUE
      M=M+MV1
    3 CONTINUE
      DO 4 I=1,MV1
      CL=C(SNEW(I))
      SIGO=SO(CL)
      ATMP=AT(TNEW(I))
      BTMP=BT(TNEW(I))
      SMT=ST(TNEW(I))
      SIGT(I)=SGT(SMT)
      T(I)=TNEW(I)
```

```
      S(I)=SNEW(I)
    4 CONTINUE
      DO 5 I=1,MH1
      AH(I)=0.0
      AHF(I)=0.0
      CAH(I)=0.0
      CAHF(I)=0.0
      CHC(I)=0.0
      CHF(I)=0.0
      CHIF(I)=0.0
      DI(I)=0.0
      HC(I)=0.0
      HF(I)=0.0
      HIF(I)=0.0
      ZI(I)=0.0
    5 CONTINUE
      J=MH1-(MH/4)
      DO 6 I=J,MH1
      ZI(I)=200.0
    6 CONTINUE
      TAU=0.0
      GO TO 201
  101 TAU=TAU+DTAU
      DO 102 I=2,MH1
      AHF(I)=HUF(I)
      CAHF(I)=CAHF(I)+PUF(I)
  102 CONTINUE
      J=MV1+1
      DO 103 I=2,MH
      Z=0.0
      J1=J-MV1
      TNEW(J)=AT1(Z)*T(J)+AT2(Z)*T(J1)
     1+AT3(DTAU)*2.*(T(J+1)-DZ*STGD(I))
      SNEW(J)=AS1(Z)*S(J)+AS2(Z)*S(J1)
     1+AS3(DTAU)*2.*S(J+1)
      Z=H
      J=J+MV
      J1=J-MV1
      TNEW(J)=AT1(Z)*T(J)+AT2(Z)*T(J1)
     1+AT3(DTAU)*2.*T(J-1)
      SNEW(J)=AS1(Z)*S(J)+AS2(Z)*S(J1)
     1+AS3(DTAU)*2.*S(J-1)
      J=J+1
  103 CONTINUE
      Z=0.0
      K=MVH1-MV
      J=K-MV1
      TNEW(K)=AT1(Z)*T(K)+AT2(Z)*T(J)+AT3(DTAU)*2.*
     1(T(K+1)-DZ*STGD(MH1))
      SNEW(K)=AS1(Z)*S(K)+AS2(Z)*S(J)+AS3(DTAU)*2.*S(K+1)
      Z=H
      K=MVH1
      J=K-MV1
      TNEW(K)=AT1(Z)*T(K)+AT2(Z)*T(J)+AT3(DTAU)*2.*T(K-1)
      SNEW(K)=AS1(Z)*S(K)+AS2(Z)*S(J)+AS3(DTAU)*2.*S(K-1)
      DO 105 J=2,MH
      Z=DZ
      K1=((J-1)*MV1)+2
      K2=(J*MV1)-1
      DO 104 K=K1,K2
      J1=K-MV1
      TNEW(K)=AT1(Z)*T(K)+AT2(Z)*T(J1)+AT3(DTAU)*
     1(T(K-1)+T(K+1))
      SNEW(K)=AS1(Z)*S(K)+AS2(Z)*S(J1)+AS3(DTAU)*
     1(S(K-1)+S(K+1))
      Z=Z+DZ
  104 CONTINUE
  105 CONTINUE
      K1=1+(MVH1-MV)
      K2=MVH1-1
      Z=DZ
      DO 106 K=K1,K2
```

```
      J=K-MV1
      TNEW(K)=AT1(Z)*T(K)+AT2(Z)*T(J)+AT3(DTAU)*
     1(T(K-1)+T(K+1))
      SNEW(K)=AS1(Z)*S(K)+AS2(Z)*S(J)+AS3(DTAU)*
     1(S(K-1)+S(K+1))
      Z=Z+DZ
  106 CONTINUE
  201 J=1
      DO 213 I=2,MH1
      J=J+MV1
      J3=J+MV
      MELT=0
      HIF(I)=0.0
      THF=DZ/2.*(T(J)-TNEW(J))
  202 CL=C(SNEW(J))
      TF(I)=F(CL)
      TTEMP=TNEW(J)
      IF(TTEMP.LE.TF(I))TTEMP=TF(I)
      TIF=DZ/2.*(TF(I)-TNEW(J))
      IF(TTEMP.GT.TF(I).AND.(ZI(I).LE.ERR(DTAU)))TIF=0.0
      CP=SH(SNEW(J))
      SIGC=SG(CL)
      ATMP=AT(TTEMP)
      BTMP=BT(TTEMP)
      SMT=ST(TTEMP)
      SIGT(J)=SGT(SMT)
      RHO=DE(SIGT(J))
      ZKW=RHO*CP/DTAU
      SRATIO=SALI/SNEW(J)
      HS=HC*(1.0-SRATIO)
      HICE=(TIF*ZKW)/(RHO1*HS)
      GO TO 204
  203 HICE=-(ZI(I)/DTAU)
      TIF=HICE*RHOI*HS/ZKW
  204 G1=-(DTAU*HICE)
      IF(G1.GT.ZI(I))GO TO 203
      DSALT=RHOI*(SNEW(J)-SALI)
      ZICE=DTAU*HICE
      SSFLUX=R(ZICE)
      SSCHG=SSFLUX/DZ
      IF(MELT.EQ.0)GO TO 206
      SDIST=SSCHG/JSA
      K1=J+(JSA-1)
      DO 205 K=J,K1
      SNEW(K)=SNEW(K)+SDIST
  205 CONTINUE
      GO TO 207
  206 SNEW(J)=SNEW(J)+SSCHG
  207 TNEW(J)=TNEW(J)+(TIF*2./DZ)
      ZI(I)=ZI(I)+DTAU*HICE
      IF(ZI(I).LT.ERR(DTAU).AND.(HICE.LE.0.0))ZI(I)=0.0
      HIF(I)=HIF(I)+TIF*ZKW
      IF(ABS(HICE).GT.EPS)GO TO 202
      CL=C(SNEW(J))
      TF(I)=F(CL)
      DO 208 K=J,J3
      CL=C(SNEW(K))
      SIGC=SG(CL)
      ATMP=AT(TNEW(K))
      BTMP=BT(TNEW(K))
      SMT=ST(TNEW(K))
      SIGT(K)=SGT(SMT)
  208 CONTINUE
      IF(MELT.EQ.1)GO TO 212
      J2=J3+1
  209 DO 210 K=1,MV
      IF(SIGT(J2-K).GE.SIGT(J3-K))GO TO 210
      L=J2-K
      CALL OVRTRN (J,L)
      GO TO 209
  210 CONTINUE
      CL=C(SNEW(J))
```

```
      TF(I)=F(CL)
      IF(TNEW(J).LE.TF(I))GO TO 212
      IF(ZI(I).LE.ERR(DTAU))GO TO 212
      MELT=1
      DO 211 K=1,MV
      IF(SNEW(J+K).EQ.SNEW(J))GO TO 211
      JSA=K
      GO TO 202
  211 CONTINUE
      JSA=MV1
      GO TO 202
  212 DI(I)=HIF(I)/(RHOI*HS)
      CHIF(I)=CHIF(I)+HIF(I)*DTAU
      HF(I)=THF*ZKW
      CHF(I)=CHF(I)+HF(I)*DTAU
      AH(I)=AHF(I)-HF(I)
      CAH(I)=CAH(I)+DTAU*AH(I)
      HC(I)=HF(I)-HIF(I)
      CHC(I)=CHF(I)-CHIF(I)
  213 CONTINUE
      I1=MV1+1
      DO 301 I=I1,MVH1
      T(I)=TNEW(I)
      S(I)=SNEW(I)
  301 CONTINUE
      J=MV1+1
      DO 403 I=2,MH1
      RHO=DE(SIGT(J))
      CP=SH(S(J))
      VEC=VTK*RHO*CP
      IF(ZI(I).LE.ERR(DTAU))GO TO 401
      TI=TF(I)
      CI=CO+BTC*SI/TI
      GRADI=DTEMP/ZI(I)
      QI=CI*GRADI
      TGRADS=QI/VEC
      TGRADL=0.0
      TGRADR=0.35*QR/VEC
      TGOW=QS/VEC
      IF(TGRADS.GT.TGOW)GO TO 401
      GO TO 402
  401 TGRADS=QS/VEC
      TGRADL=QL*EXP(-0.5*ZI(I))/VEC
      TGRADR=(0.35*QR+0.65*QR*EXP(-0.5*ZI(I)))/VEC
  402 STGD(I)=TGRADS+TGRADL+TGRADR
      HUF(I)=STGD(I)*VEC
      PUF(I)=HUF(I)*DTAU
      J=J+MV1
  403 CONTINUE
      IF(AMOD(TAU,3600.).LT.1.E-4) GO TO 501
      GO TO 101
  501 J1=1
      TIME=TAU/3600.
      J2=MVH1-MV
      WRITE(6,200)TIME,IRUN
      WRITE(6,250)(TF(K),K=1,MH1)
      DO 502 I=1,MV1
      WRITE(6,300)(T(J),J=J1,J2,MV1)
      WRITE(6,350)(S(J),J=J1,J2,MV1)
      WRITE(6,400)(SIGT(J),J=J1,J2,MV1)
      J1=J1+1
      J2=J2+1
  502 CONTINUE
      WRITE(6,450)
      DO 503 I=2,MH1
      WRITE(6,500)HIF(I),CHIF(I),DI(I),ZI(I),HC(I),CHC(I),
     1HF(I),CHF(I),AH(I),CAH(I),AHF(I),CAHF(I)
  503 CONTINUE
      IF(TIME.GE.48.)GO TO 1
      GO TO 101
  100 FORMAT(I2)
  150 FORMAT(11F7.2)
```

```
  200 FORMAT('1','PROFILE (X-Z PLANE) OF LEAD AT TIME=',F5.1
     1,10X,'RUN NUMBER',I3)
  250 FORMAT('0','TF',3X,21(1X,F5.2))
  300 FORMAT('C','T',4X,21(1X,F5.2))
  350 FORMAT(' ','S',4X,21(1X,F5.2))
  400 FORMAT(' ','ST',3X,21(1X,F5.2))
  450 FORMAT(//,'0',3X,'HIF',7X,'CHIF',6X,'DI',8X,'ZI',8X,
     1'HC',8X,'CHC',7X,'HF',8X,'CHF',7X,'AH',8X,'CAH',7X,
     2'AHF',7X,'CAHF',/)
  500 FORMAT(' ',1PE9.2,11(1X,E9.2))
 1000 STOP
      END


      SUBROUTINE CVRTRN (I,K)
      COMMON TNEW(232),SNEW(232),SIGT(232)
      C(A)=(A-0.030)/1.8050
      SO(A)=-0.069+1.4708*A-0.001570*A**2+0.0000398*A**3
      AT(A)=A*(4.7867-0.098185*A+0.0010843*A**2)*0.001
      BT(A)=A*(18.030-0.8164*A+0.01667*A**2)*0.000001
      ST(A)=-(A-3.98)**2/503.570*(A+283.)/(A+67.26)
      SGT(A)=A+(SIGO+0.1324)*(1.0-ATMP+(BTMP*(SIGO-0.1324)))
      K1=K-1
      J$=1
      L=0
      DO 1 M=I,K1
      L=L+1
      IF(SIGT(K-L).GE.SIGT(K))GO TO 1
      L1=1+(K-L)
      J$=2
      GO TO 2
    1 CONTINUE
    2 CTEMP=0.0
      CSALT=0.0
      IF(J$.EQ.1)L1=I
      DO 3 N=L1,K
      CTEMP=CTEMP+TNEW(N)
      CSALT=CSALT+SNEW(N)
    3 CONTINUE
      NN=1+(K-L1)
      ATEMP=CTEMP/FLOAT(NN)
      ASALT=CSALT/FLOAT(NN)
      CL=C(ASALT)
      SIGO=SO(CL)
      ATMP=AT(ATEMP)
      BTMP=BT(ATEMP)
      SMT=ST(ATEMP)
      ASIGT=SGT(SMT)
      DO 4 M=L1,K
      TNEW(M)=ATEMP
      SNEW(M)=ASALT
      SIGT(M)=ASIGT
    4 CONTINUE
      RETURN
      END
```

BIBLIOGRAPHY

Arctic Meteorology Research Group, Department of Meteorology, McGill University, Montreal, Publication in Meteorology No. 70, Scientific Report No. 12, Heat Flux Through the Polar Ocean Ice, by E. Vowinckel, 15 pp., September 1964.

Badgley, F.I., "Heat Balance at the Surface of the Arctic Ocean," Proc. Western Snow Conference, Spokane, Washington, 101-104, 1961.

Badgley, F.I., "Heat Budget at the Surface of the Arctic Ocean," Proc. Symp. Arctic Heat Budget and Atmospheric Circulation, The Rand Corporation, RM-5233-NSF, 267-277, 1966.

Baffin Bay-North Water Project Scientific Report No. 1, The Physical Oceanography of the Northern Baffin Bay Region, by R.D. Muench, 150 pp., The Arctic Institute of North America, January 1971.

Bilello, M., "Formation, Growth and Decay of Sea Ice in the Canadian Arctic Archipelago," Arctic, v. 14, 3-24, March 1961.

Bryan, K., "Climate and the Ocean Circulation, Part III: The Ocean Model," Monthly Weather Review, v. 97, 806-827, November 1969.

Coachman, L.K., "Production of Supercooled Water During Sea Ice Formation," Proc. Symp. Arctic Heat Budget and Atmospheric Circulation, The Rand Corporation, RM-5233-NSF, 497-529, 1966.

Coachman, L.K. and Barnes, C.A., "The Contribution of Bering Sea Water to the Arctic Ocean," Arctic, v. 14, 147-161, September 1961.

Coachman, L.K. and Barnes, C.A., "Surface Water in the Eurasian Basin of the Arctic Ocean," Arctic, v. 15, 251-277, December 1962.

Doronin, Y.P., "Characteristics of the Heat Exchange," Proc. Symp. Arctic Heat Budget and Atmospheric Circulation, The Rand Corporation, RM-5233-NSF, 247-266, 1966.

Fletcher, J.O., "The Arctic Heat Budget and Atmospheric Circulation," Proc. Symp. Arctic Heat Budget and Atmospheric Circulation, The Rand Corporation, RM-5233-NSF, 23-43, 1966.

Foster, T.D., "Haline Convection Induced by the Freezing of Sea Water," Jour. Geophys. Res., v. 73, 1933-1938, March 1968.

Foster, T.D., "Experiments on Haline Convection Induced by the Freezing of Sea Water," Jour. Geophys. Res., v. 74, 6967-6974, December 1969.

Knudsen, M., Hydrographical Tables, p. I-V, reprinted by Tutein and Koch, Copennagen 1959, 1902.

Lake, R.A. and Lewis, E.L., "Salt Rejection by Sea Ice During Growth," Jour. Geophys. Res., v. 75, 583-597, January 1970.

Lewis, E.L. and Walker, E.R., "The Water Structure Under a Growing Sea Ice Sheet," Jour. Geophys. Res., v. 75, 6836-6845, November 1970.

Manabe, S., "Climate and the Ocean Circulation, Part I: The Atmospheric Circulation and the Hydrology of the Earth's Surface; Part II: The Atmospheric Circulation and the Effect of Heat Transfer by Ocean Currents," Monthly Weather Review, v. 97, 739-805, November 1969.

Maykut, G.A. and Untersteiner, N., Numerical Prediction of the Thermodynamic Response of Arctic Sea Ice to Environmental Changes, 173 pp., The Rand Corporation, RM-6093-PR, November 1969.

Maykut, G.A. and Untersteiner, N., "Some Results from a Time-Dependent Thermodynamic Model of Sea Ice," Jour. Geophys. Res., v. 76, 1550-1575, February 1971.

Pounder, E.R., The Physics of Ice, pp. 125-127, Pergamon, 1965.

Smith, G.D., Numerical Solution of Partial Differential Equations, pp. 70-71, Oxford University, 1965.

Stern, M.E. and Turner, J.S., "Salt Fingers and Convecting Layers," Deep Sea Research, v. 16, 497-511, 1969.

Sverdrup, H.U., Johnson, M.W. and Fleming, R.H., The Oceans, p. 61, 66, Prentice-Hall, 1942.

Untersteiner, N., "Calculating Thermal Regime and Mass Budget of Sea Ice," Proc. Symp. Arctic Heat Budget and Atmospheric Circulation, The Rand Corporation, RM-5233-NSF, 203-213, 1966.

U.S. Naval Civil Engineering Laboratory Technical Report R-497, Ice Engineering - Analysis of the Growth of Sea Ice, by A.J. Mettler and N.S. Stehle, 46 pp., November 1966.

INITIAL DISTRIBUTION LIST

		No. Copies
1.	Defense Documentation Center Cameron Station Alexandria, Virginia 22314	2
2.	Dr. Ned A. Ostenso Office of Naval Research, Code 480D Arlington, Virginia 22217	1
3.	U.S. Naval Arctic Research Laboratory Attention: Librarian Barrow, Alaska 99723	1
4.	The Arctic Institute of North America 1619 New Hampshire Avenue, NW Washington, D.C. 20009	1
5.	University of Michigan Attention: Library Ann Arbor, Michigan 48108	1
6.	Library, Code 0212 Naval Postgraduate School Monterey, California 93940	2
7.	Department of Oceanography Naval Postgraduate School Monterey, California 93940	3
8.	Asst Professor J.A. Galt, Code 58Gl Department of Oceanography Naval Postgraduate School Monterey, California 93940	8
9.	LCDR Richard H. Schaus, USN P.O. Box 1127 Carmel, California 93921	2

Security Classification

DOCUMENT CONTROL DATA - R & D

(Security classification of title, body of abstract and indexing annotation must be entered when the overall report is classified)

1. ORIGINATING ACTIVITY (Corporate author)

Naval Postgraduate School
Monterey, California 93940

2a. REPORT SECURITY CLASSIFICATION

Unclassified

2b. GROUP

3. REPORT TITLE

A Thermodynamic Model of a Central Arctic Open Lead

4. DESCRIPTIVE NOTES (Type of report and, inclusive dates)

Master's Thesis: September 1971

5. AUTHOR(S) (First name, middle initial, last name)

Richard Harris Schaus

6. REPORT DATE	7a. TOTAL NO. OF PAGES	7b. NO. OF REFS
September 1971	86	25

8a. CONTRACT OR GRANT NO.	9a. ORIGINATOR'S REPORT NUMBER(S)
b. PROJECT NO.	
c.	9b. OTHER REPORT NO(S) (Any other numbers that may be assigned this report)
d.	

10. DISTRIBUTION STATEMENT

This document has been approved for public release and sale;
its distribution is unlimited.

11. SUPPLEMENTARY NOTES	12. SPONSORING MILITARY ACTIVITY
	Naval Postgraduate School Monterey, California 93940

13. ABSTRACT

A time-dependent, two-dimensional thermodynamic model of an open lead in central arctic sea ice is presented. The model is generated by opening a lead of finite width and infinite extent in the equilibrium sea-ice cover. From this initial condition, the model is integrated numerically as a sea-ice cover is reestablished over the lead. The effects of various representative advective parameterizations, and temperature and salinity profiles in the ocean's surface layer, on the heat flux through the lead and on the nature of ice formation are investigated as the lead closes by thermal processes alone. Continuity equations involving a horizontal advection term and a vertical diffusion term govern heat and salt transport in the water. Cooling-induced convective overturn as a mechanism for vertical heat and salt transport in the water column is treated through an artifice of the vertical diffusion term.

DD FORM 1 NOV 65 1473 (PAGE 1)

S/N 0101-807-6811

Security Classification

-31408

KEY WORDS	LINK A		LINK B		LINK C	
	ROLE	WT	ROLE	WT	ROLE	WT
Arctic						
Sea Ice						
Heat Budget						
Air-Sea Budget						
Numerical Model						
Lead						
Polynya						

7 FEB 73
BINDERY
21368
22754
22754
26101

Thesis 130716
S28 Schaus
c.1 A thermodynamic model of a central Arctic open lead.